**Title**
Ignition Capability of Mechanically Generated Sparks Landing in Fuel Beds

**Permalink**
https://escholarship.org/uc/item/69f2k6ns

**Author**
Antunez, Salvador

**Publication Date**
2018

Peer reviewed|Thesis/dissertation

UNIVERSITY OF CALIFORNIA
RIVERSIDE


Ignition Capability of Mechanically Generated Sparks
Landing in Fuel Beds


A Thesis submitted in partial satisfaction
of the requirements for the degree of


Master of Science


in


Mechanical Engineering


by


Salvador Antunez


March 2018


Thesis Committee:
        Dr. Marko Princevac, Chairperson
        Dr. Guillermo Aguilar
        Dr. David Weise

The Thesis of Salvador Antunez is approved:

_____

_____

_____
                                    Committee Chairperson

University of California, Riverside

# Acknowledgments

A great number of people have provided me with help and support in completing this thesis.

In particular, I would like to thank:

- Dr. Marko Princevac, my supervisor, and mentor for this thesis, who provided valuable advice in relation to the methodology and the content of the thesis.

- The staff of the USDA Forest Service Pacific Southwest Research Station, Riverside, California laboratory and specifically Dr. David Weise, Ms. Gloria Burke, Ms. Bonni Corcoran, and Mr. Joey Chung who contributed enormously to the experimental part of this project.

- My friends and lab members of the Laboratory For Environmental Flow Modeling from the Department of Mechanical Engineering, University of California, Riverside, most especially Jeanette Cobian , AmirHessam Aminfar , Aliasgar Badani, Noah Yim, Santiago Kirchfeld, Matthew Choi, Jon Josey

- Sam Wu, project manager, who funded the project through the prestigious grant: US DEPARTMENT OF AGRICULTURE FOREST SERVICE, 16RD-1113-8100-024

- Finally, I would like to thank my family and friends for their constant support and never-ending patience.

# Dedication

My mother, Carolina Antunez Zaragoza, who has supported and encouraged me to strive for a better life and achieve such great success and honor.

My father, Adislao Antunez Navor, who has made an honest living for us and has always placed his family before himself.

My little brother, Ivan Antunez, who has stood strong during my departure and hope the completion of this thesis serves as a great inspiration.

ABSTRACT OF THE THESIS

Ignition Capability of Mechanically Generated Sparks
Landing in Fuel Beds

by

Salvador Antunez

Master of Science, Graduate Program in Mechanical Engineering
University of California, Riverside, March 2018
Dr. Marko Princevac, Chairperson

The primary focus of this study is to analyze the ignition capability of different metal particles and how a shower of metal particles generated from grinding can cause ignition of wildland fuels. To this end, this thesis focuses on describing the experimental apparatus and procedures developed to investigate the ignition capability of different metals in combination with different wildland fuels. Moreover, the experimental data results are presented in a manner to improve future analytical and numerical models. A detailed thermal and statistical analysis will be included as a part of the full project report. The experiments were performed using three different type of metals which are stainless steel, copper, and cold rolled steel. The grinding of these materials generated hot particles that were directed downwards into a collection box containing wildland fuels. The fuels consist of the following: Lehmann lovegrass, wildoats, timothy grass and cheatgrass. For the first set of experiments, the interaction between the metals and fuels at different fuel temperatures were studied. It was found that cold rolled steel and stainless-steel particles

possessed the highest ignition capabilities. For the second set of experiments, the fuel

moisture was varied considerably (20% - 80%), and it was determined that cold rolled steel

particles could considerably ignite the fuels at high fuel moisture percentages. For the last

set of experiments, the distance between the fuel bed and grinder was varied to match that

of real-life applications. It was concluded that cold rolled steel could ignite fuels up to

distances of 100 cm. For all metals, particles were collected and examined under a

microscope at 400x magnification. Results indicate that the diameter of the particles from

cold rolled and stainless steel ranged from 0.0625 mm to 0.80 mm and were considerably

smaller than that of copper, which ranged from 0.4375 mm to 2.5 mm. Physical processes

conclude that cold rolled steel and stainless steel achieve higher initial temperatures than

those of copper due to differences in the toughness of the material. The tougher metals

absorb a higher amount of separation energy before fracture and increase the probability

of the particles combusting.

# Table of Contents

# List of Figures

xii

# List of Tables

# Nomenclature

**English**

A      surface Area

$c$      specific heat of the body

d      diameter

$\bar{h}$      convective heat transfer coefficient

$k$      thermal conductivity

$Nu$      Nusselt Number

$Pr$      Prandtl Number

$Re$      Reynolds number

$T$      temperature

$t$      time

U      velocity

V      volume

**Greek**

$\varepsilon$      emissivity

$\mu$      dynamic viscosity

$\rho$      density

$\nu$      kinematic viscosity

$\sigma$      Stefan-Boltzmann constant

# 1.0 Introduction

Wildland fires have existed for centuries and are only expected to increase due to global warming. This specifically affects the western US, in which fires have been occurring "five times more often than the 1970 and 80s and are burning more than six times the land area" (Brandin, 2017). These continuing climate changes will only continue to make the wildland fuels drier; consequently, increasing ignition probability. Not only do these catastrophic fires risk the lives of citizens and firefighters but they can also destroy nearby properties, national forests, and habitats inhabited by animals. Recent wildfires include the 2017 Northern California Wildfires and the 2017 Thomas Fire (Southern California). The Thomas Fire was recorded as the 5th largest wildfire in modern California history and burned over 230,000 acres (Yan *et al.,* 2017).

Wildfires require three drivers to start and spread: oxygen, fuel and an ignition source. Potential ignition sources are the following: arsonist, lightning, campfires, and mechanical equipment use. Mechanical equipment operations such as welding, and grinding have been documented as one of the causes of wildfires. From Figure 1.1, we can see that mechanically generated sparks account for about seven percent of wildfires that occur yearly (Ignition Sources, 2015).
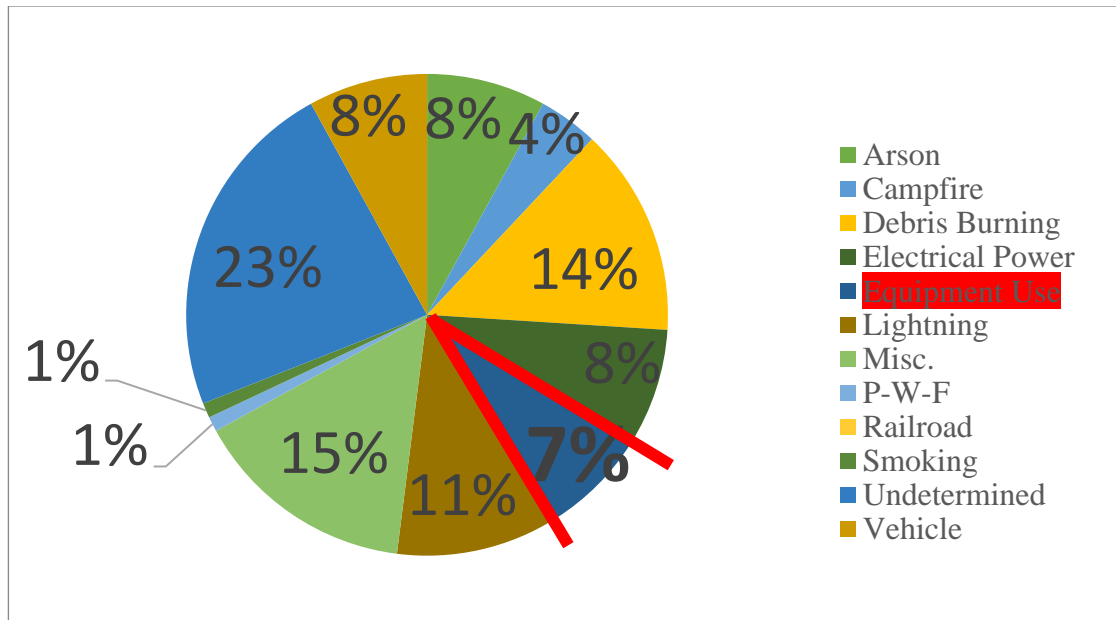
**Figure 1.1** Ignition Sources. Acquired from Ignition Sources California 2015 (CalFire)

Mechanically generated sparks are characterized as external sources which act as delivery agents of heat. The probability of ignition is highly dependent on not only the metal's thermal (*i.e*., thermal conductivity, melting point, etc.) and mechanical properties (toughness, the percentage of carbon, etc.) but also on the fuel's properties (fuel moisture content, density, etc.). Understanding how the combination of these properties may result in the ignition of wildland fuels is an important consideration in reducing wildfires.

According to Fernandez-Pello *et al.* (2015), they hypothesize that the accumulation of these particles is required for ignition. Unfortunately, ignition of fuel beds by multiple sparks is difficult to understand because of the multiple influential factors that affect ignition, which was mentioned above. Consequently, several groups have studied the

ignition of wildland fuels by a single hot metal particle at larger sizes ($\geq$ 0.8m). Investigations most relevant to our work are discussed here.

Babrauskas (2003) presented results on the spark generation potential from various metals in two categories: high spark potential and low spark potential. These results are presented in Table 1.1. It is important to note that sparks are not present during the grinding of aluminum, copper, and magnesium. Finney *et al.* (2013) studied the potential of rifle bullets to ignite wildland fuels. The physical process of how the rifle bullets acquired sufficient thermal energy to ignite the fuels was very similar to the physical mechanisms behind our study. They found that the material of the bullet influenced the ignition potential due to the different temperatures achieved by the fragments after impact. It was found that the larger particles more easily facilitated ignition. Howitt (2015) conducted a similar study on the physical process of the ignition potential of hot metal fragments from heavy mechanical equipment. It was found that the fragments did not reach sufficient temperatures to ignite wildland fuels. A numerical study was performed by Tse and Fernandez Pello (1997) on the flight path of metal particles created from arcing power lines. When considering the same size metal particles, they found that the copper particles can deliver a higher amount of heat than the aluminum particles but travel a smaller distance. Unlike copper particles which do not emerge burning, the larger aluminum particles have the potential of landing while still burning. Hadden *et al.* (2011) studied the ignition of combustible fuel beds by hot particles. Results show that the larger heated spheres require less temperature to ignite the fuels when compared to smaller size spheres. Similarly, Wang *et al.* (2013) conducted a study on the ignition potential of molten copper

beads as they fell from a height of 0.02 m to 1.0 m. This simulated the flight path of a

molten particle landing in a fuel bed after being ejected from a short circuit box.

**Table 1.1** Sparking Potential of Various Elements

| High Sparking Potential | Low Sparking potential |
|---|---|
| Calcium, carbon, cerium, iron, nickel, potassium | Aluminum, beryllium, cadmium, copper, gold, lead, magnesium, palladium, silver, tin, zinc. |

Furthermore, Zak *et al.* (2014) researched the ignition capability of aluminum and

steel particles landing in cellulose fuels bed. They found that spheres with diameters below

2.38 mm or 2.03 mm for aluminum did not ignite cellulose. Moreover, temperatures up to

1100 ℃ did not produce ignition either. They also observed that aluminum spheres, with

diameters from 4 mm to 8 mm, have a higher ignition capability than stainless steel. This

was supported by the fact that aluminum melts at a 660 ℃ and acquires more energy than

stainless steel from its melting. Moreover, Schlieren images showed that a hot gas contour

expands away from the sphere when ignition occurs. This indicates the production of

gaseous pyrolyzate, generated by the process of the sphere heating the cellulose fuel bed.

Similar to the work of Hadden *et al.* (2011) and Zak *et al.* (2014), the potential to

ignite natural fuel beds by hot metal particles, embers, and sparks was studied by

Fernandez-Pello *et al.*, (2015). Fernandez-Pello's work aligned with Hadden's finding on

how larger particles require a lower temperature to ignite fuel beds than the smaller

particles. More importantly, they showed that the energy and temperature of the particle

are more significant factors than its thermal properties when determining ignition. For

smaller particles, it was shown that the energy of the particle is more important than the temperature of the particle. Also, they postulated that the accumulation of sparks must occur for ignition to occur. However, they state that further research must be conducted to analyze this phenomenon further.

Manzello *et al.* (2006) conducted a study on the ignition of fuel beds by the following two firebrands: 1) glowing firebrands and 2) flaming firebrands. The main purpose of this study was to build an apparatus that achieved the results mentioned. They reported that it was possible to ignite shredded paper beds from single glowing and flaming firebrands. This suggests that it is possible to ignite home attics under a similar process.

Kaminski (1974) studied the potential of starting a fire using a chainsaw equipped with spark arrestors. It was determined that the chainsaw spark arrester possess the ability to ignite fuels upon contact. The restricting exhaust flow produced by the muffle/arrester heats up the arrester to temperatures high enough to ignite fuels. For safe operations, it was proposed that the shell temperature remains below 260 °C and the gaseous exhaust temperature not exceed 232 °C.

Pitts (2007) conducted experiments on the study of ignition of grasses by conduction or radiation. The experiments were designed to replicate ignition of fuels by heated mufflers and catalytic converters. They found that increased wind speed decreased ignition time of fuels. Consequently, higher heated plate temperature was required for ignition to occur in the absence of wind.

Hawksworth *et al.* (2006) assessed the ignition potential of mechanical equipment. They found that the probability of ignition by hot surfaces is dependent on the power, load,

speed, size, and coefficient of friction produced by the equipment. An increase in the coefficient of friction and an increase in speed will both result in higher temperatures with a larger volume of sparks. They used these parameters to suggest possible approaches for ignition potential by mechanical equipment.

Plucinski and Anderson (2008) researched the following factors affecting ignition in litter fuels: the presence of litter type, wind, fuel moisture content, and ignition source. They found that the litter characteristics, such as bulk density and surface area to volume ratio played a key role in determining ignition. Also, they stated that the addition of wind decreased, or increased, ignition based on where the ignition source was located (top or bottom of fuel). The fuel moisture content was the most crucial factor in determining ignition and varied with success depending on the other parameters.

Several studies have focused or dealt with particle diameters ranging above 0.8 mm, but very few studies have analyzed how particles at the microscale size may cause ignition of wildland fuels. Behrend and Ritter (2004) studied how mechanically generated sparks at the microscale size may potentially ignite explosion-hazard areas such as gas-air mixtures. It was found that the size and temperature of the particle strongly rely on the material properties and the amount of deformation energy that was absorbed before fracture. The study of sparks produced from the abrasion of titanium alloys in golf club heads (Arulmoli *et al.*, 2014) further supports that micro size particles do possess the ignition capability to ignite dry grasses.

A major advance in wildfire research would be the development of both an analytical and numerical model to predict the ignitability of wildland fuels due to a shower

of hot metal sparks. Some models have been published (Tse *et al.*, 1998), which determine the particle temperature right before impact with the fuel but lack the incorporation of how other parameters (fuel moisture, material type, etc.) play a key role in determining ignition. Therefore, a detailed experimental study of assessing the ignition capability of mechanically generated sparks is required to improve such models.

Consequently, the primary focus of this study is to analyze the ignition capability of different metal particles and how a shower of metal particles generated from grinding can cause ignition of wildland fuels. To this end, this thesis focuses on describing the experimental apparatus and procedures developed to investigate the ignition capability of different metals in combination with different wildland fuels. Moreover, the experimental data results are presented in a manner to improve future analytical and numerical models. A detailed thermal and statistical analysis will be included as a part of the full project report. The apparatus allowed the metal workpiece to impact the grinder and deflect the generated shower of sparks onto the fuel bed. The ability to deflect the shower of sparks onto the fuel is important, as it is speculated that the accumulation of energy from multiple particles (sparks) is required for ignition to occur. The metals considered were copper, stainless steel and cold rolled steel and the fuels considered were Lehmann lovegrass, Wild oats, Timothy grass, and Cheatgrass. The parameters varied were the fuel temperature, fuel moisture and the distance from the grinder to the fuel bed. The fuel temperature was varied to match that of moderate and hot summer conditions, and the distance was varied to replicate real-life applications. Finally, the experimental results presented here were

supported by relevant studies and are hope to be used to improve future analytical and numerical models.

# 2.0 Experimental Methods

In the following section, the experimental apparatus designed for the work is presented here.

## 2.1 Experimental Apparatus

The following experimental apparatus was used in the grinding ignition study, which can be seen in Figure 2.1. A more detailed schematic of the apparatus can be seen in Figure 2.3, referencing the SolidWorks drawings provided to the manufacturer. The grinding ignition test rig consists of 80/20 aluminum T-slotted frames that were manufactured by 80/20 Inc., modified and assembled in the fire laboratory at the USDA, Forest Service Southwest Research Station. The experimental tests were conducted by fixing a handheld angle grinder to the test rig, which was designed to apply a constant pressure between the metal workpiece and the grinding wheel. The angle grinder was orientated at a thirty-degree angle to best replicate real-world applications. The generated sparks were directed toward the fuel bed, which was placed a set distance directly below the grinding wheel. Upon contact, the generated sparks could potentially ignite the fuel bed. For our study, the 80/20 aluminum T-slotted frame design was chosen, since it offered many advantages to our proposed work. The aluminum frames were light in weight, and the T-slots allowed the frames to be easily modified in either the x or y distance. The simple T-slot design allowed for external attachments, which were used to hold the metal workpiece and the grinder in place. The slider mechanism, which held the metal workpiece in place, allowed the

workpiece to be fed into the grinder. The slider mechanism was modified for safety reasons

by adding an external metal piece as a cover which was securely tightened by a bolt. The

grinder was held by L-shape brackets which were attached to the side of T-slot frames.

(Refer to Figure 2.1 and Figure 2.3 for more details).
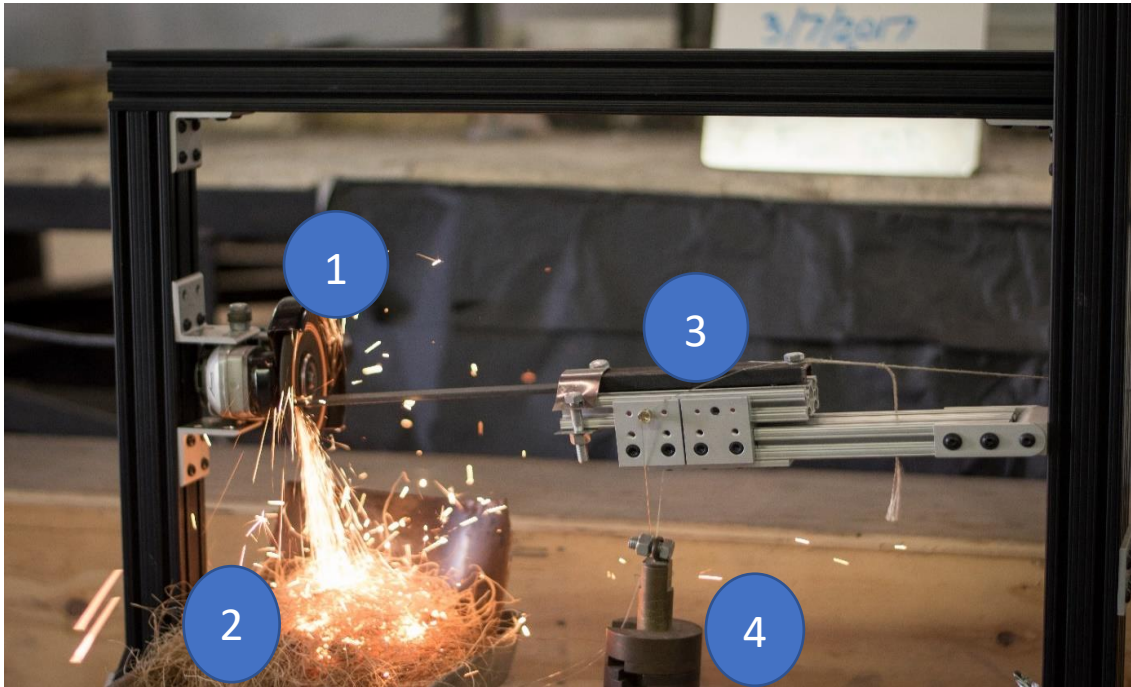


**Figure 2.1** Image of T-slot Experimental Apparatus. (1): Angle grinder secured onto side of T-slot frames by L-shaped brackets; (2): Sparks impacting fuel bed at a set distance right underneath angle grinder; (3): Slider mechanism, which allows the workpiece to be fed into angle grinder (4): Weights acting as a pulley system to move sliding mechanism

**Figure 2.2** Ignited Fuel Bed After Experiment Using T-Slot Apparatus
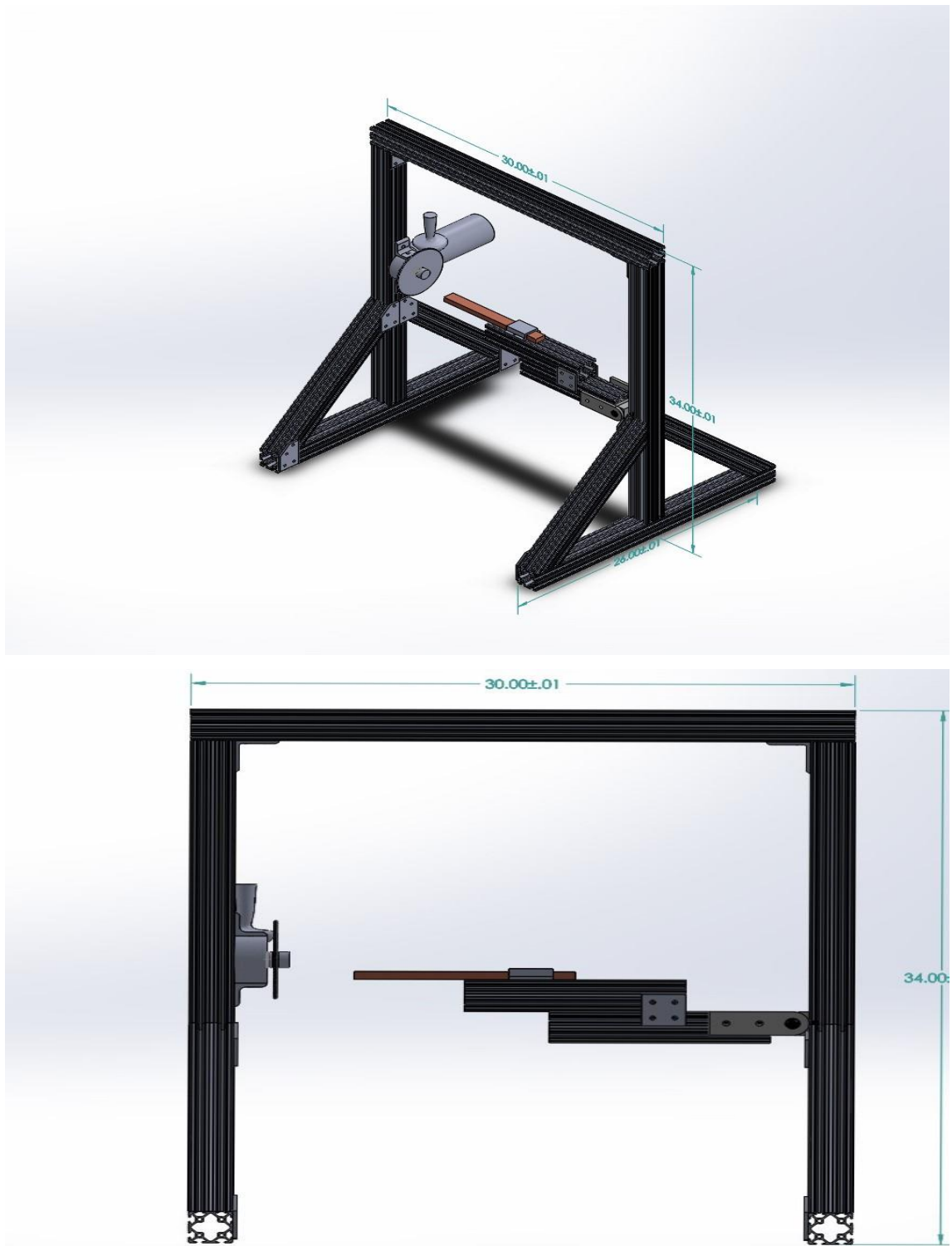
**Figure 2.3** Solidwork Drawings of Apparatus

The T-slotted experimental apparatus was initially designed to eliminate random variables that could affect the results of the experiment, such as, the user shaking or exerting a different pressure when grinding. Although successful, the loading and unloading of the metal workpiece proved to take a significant amount of time. Hence, the apparatus was substituted for a more efficient but elementary design (refer to Figure 2.4). The metal workpiece was held in position by a 6-inch adjustable bench vice which was securely tightened onto the cinderblocks with C-clamps. In addition to making the experiment safer, the bench vice provided flexibility in that workpiece of different sizes or shapes (flat or round bar) could be ground. The user could easily adjust the distance from the fuel tray to the grinder by adding or removing cinderblock(s). The procedure was the same in that the user would begin grinding for a total of five minutes until ignition was observed. Overall, the design proved to be more time efficient when replacing the workpiece with a new material and allowed for a greater number of experiments to be conducted in a day.
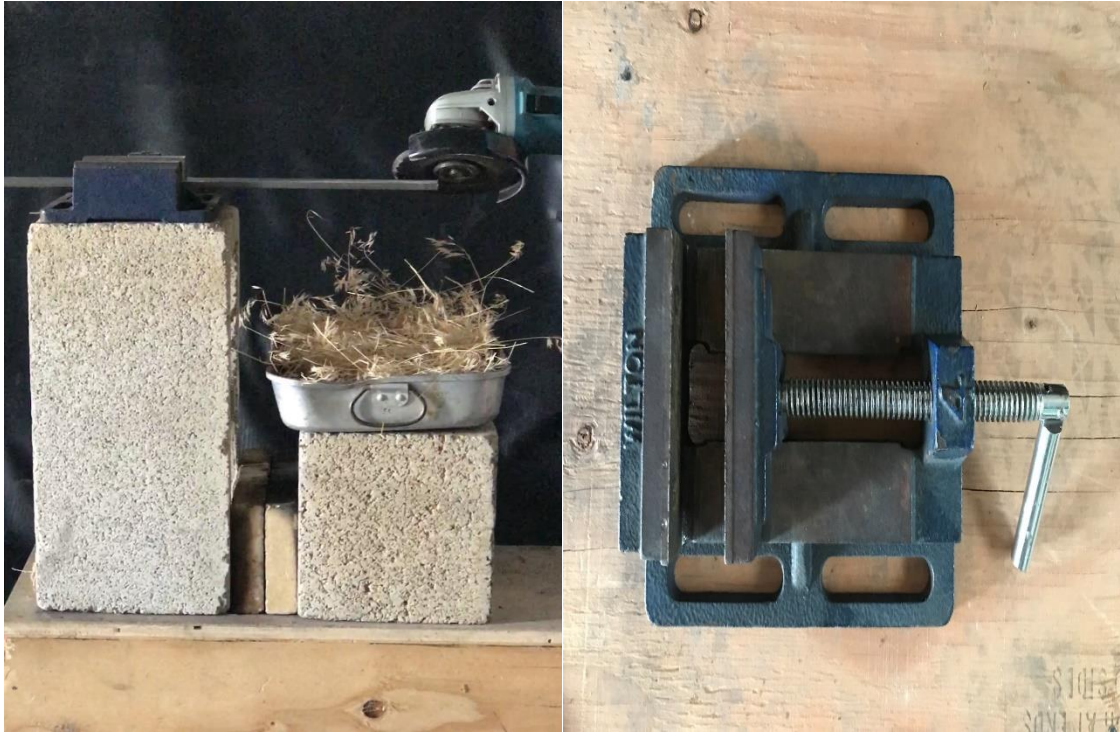
**Figure 2.4** Images of New Experimental Apparatus. Simple design in which an adjustable 6-inch bench vise holds the metal workpiece in position and angle grinder is held by the user. A 9.5 by 13-inch fuel tray is placed directly in the path of the mechanically generated sparks. The distance may easily be adjusted by adding or removing cinderblock(s).

## 2.2 Experimental Procedure

For each general experiment, 35 grams of the desired fuel was weighed and placed on an aluminum tray. From the same batch of fuel, approximately 5 grams was trimmed and loaded onto the Computrac 2000XL. The Computrac 2000XL is a moisture analyzer that provides the dry-weight fuel moisture. It does so by using "the proven loss-on-drying method to detect the volatile content of a sample of test material" (Computrac User Manual, 1996). Also, the ambient temperature and relative humidity were measured before every experiment using a Kestrel Environmental meter. After loading of the fuel, the fuel tray

was then placed a set distance, which was determined from the top of the fuel to the top of the material being ground. The top of the fuel is where the particles/sparks first contact the fuel, and the top of the material is where the grinding disk first contacts the material (grinding cutting zone). The desired metal workpiece being ground was placed and secured onto the bench vise holder. The material was designated to extend outwards to a distance that matched the whole width of the bed, as for some experiments (copper) this is critical. There was no control of where the sparks first impacted the fuel or how deep the sparks penetrated the fuel. This was all randomized as it varied with the fuel bed characteristics (density, packing) and the metal workpiece being ground. An effort was made to stay consistent in how every material was ground. The videography which consisted of the high-speed camera, infrared camera, and video recorder were all set up and began recording upon instruction. Grinding of the material started as soon as the videography started recording. Simultaneously, a stopwatch was started for verification of ignition times. For non-ignition trials, a maximum time of 5 minutes was set as a time limit, at which point and time the user stopped grinding and declared the end of the experiment. Hence, all videography and stopwatch stopped at the final time, which is determined by the two scenarios mentioned above (Ignition or No Ignition). Ignition results were recorded and classified as the following: charring, smoldering, and flaming. According to Di Blasi (1993), charring is the carbon-rich non-volatile residues after incomplete combustion of fuels when subjected to external heating. Smoldering ignition (Figure 2.5 a) follows the same initial process as flaming ignition in which fuel is exposed to external heating, but the resulting heat flux is not high enough for pyrolysis to occur (Finney *et al.*, 2016).

14

Flaming ignition (Figure 2.5 b) can be defined as when the "fuel is exposed to a heat source that provides sufficient energy to cause thermal decomposition of the material (pyrolysis)" (Finney *et al.*, 2016). Images of smoldering and flaming ignition may be seen below.



**Smoldering Ignition**                    **Flaming Ignition**

**Figure 2.5** Ignition Classification Images. Smoldering ignition on left-hand side and flaming ignition on right-hand side.

The respective time at which each classification of ignition occurred was recorded visually by the user and verified by the corresponding times recorded by the videography. The transition time from smoldering to flaming ignition was computed from this collected data. The percent of the fuel that was charred was determined visually by the user at the end of the experiment. After all data was recorded and logged, experiments were repeated in the same procedure. Further procedure details pertaining to each respective set of experiments (Set 1, 2, and 3) are explained in section 4.1 (Classification of Experiments).
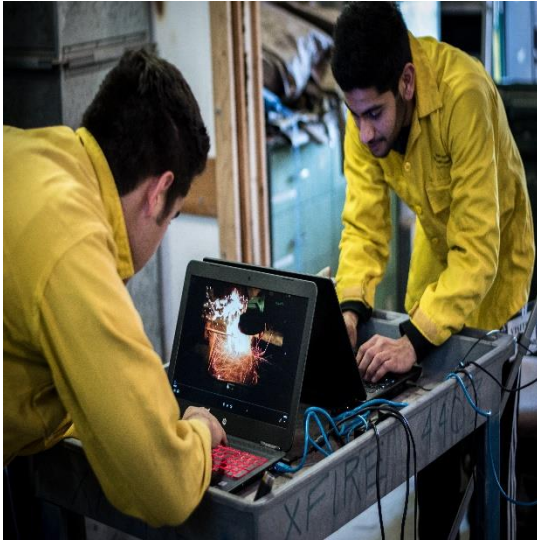
**(a)**



**(b)**



**(c)**



**(d)**

**Figure 2.6** The procedure followed during experiments. a) Setup of high speed and infrared camera, b) Data logging and measurement of fuel mass and fuel moisture, c) Fuel mass scale, d) Computrac 2000XL moisture analyzer

## 2.3 Procedure of Particle Analysis

Metal particles of copper, cold rolled steel, and stainless steel were collected in a glass jar filled with water. Upon impacting the water, the particles cooled down instantly and maintained their size. On the same day, to avoid rust, particles were filtered using a simple paper filter. The particles were then placed in a paper envelope and oven dried at 85 °C for a few hours. Lastly, each sample was observed under a microscope with a total magnification of 400x. A total of 10 samples were taken for each metal. Each sample was aligned under the microscope with the calibrated scale that enabled particle sizing. The scale was calibrated by the USDA, Forest Service Southwest Research Station staff.

## 2.4 Experimental Matrix

This section provides a brief description of the grinder, materials, and fuels used throughout the experiments.

### 2.4.1 Type of Grinder and Grinding Wheel Used

A 13-amp SJS paddle switch Makita angler grinder (Figure 2.8) was used which delivered approximately 11,500 RPM at its highest setting. The grinding wheel used for all experiments was a 5" Type 27 Aluminum Oxide depressed center wheel. Other material type grinding wheels were tested; such as Zirconia Alumina, but were deemed to have no difference on the effects of grinding.

**Figure 2.7** Makita Angle Grinder.  Image from Makitatools.com

## 2.4.2  Metals Investigated

Different metals were selected because this varied the material's mechanical and thermal properties. Copper was chosen because it can be found in clashing conductors which have been cited by Tse and Fernandez-Pello (1998) to possess the probability of starting ignition of wildland fuels. Aluminum can also be found in clashing conductors but was tested and verified that it did not spark during preliminary testing. Stainless steel and cold rolled steel was chosen because they are common materials used when machining and grinding. The following table list the dimensions of the material used consistently throughout all experiments:

**Table 2.1** Material Dimensions

| Material | Material Grade Selection | Dimensions (inches) |
|---|---|---|
| Copper | AISI 1018 Steel, Cold Drawn | ½" Round Bar |
| Stainless Steel | 304 Stainless Steel | 1/8 x 3/4 Flat Bar |
| Cold Rolled Steel | Copper Bar Alloy 110 | 1/8 x 3/4 Flat Bar |

### 2.4.3 Fuels Investigated

The following were the fuels investigated: Lehmann lovegrass, Wild oats, Timothy grass, and Cheatgrass. An effort was made to research the complex fire ecology and adaptation of all the fuels and how it related to our work.

Lehmann lovegrass (*Eragrostis lehmanniana*) is a non-native grass to the U.S. and was introduced from East Africa (Figure 2.9). It is a rapidly growing bunchgrass that reaches a height of 30 to 40 inches. Lovegrass serves as a habitat for some animals or as a food source for others. Lehmann lovegrass is reported to have heavy accumulations of dead fuel at the base of the plant; thus, increasing the chances of wildfires. Additionally, this grass sprouts fast and colonizes after burning (USDA NRCS Plants Material Program, 2002). Lehmann lovegrass was readily available at the USDA, Forest Service Southwest Research Station and was initially collected in Fort Huachuca, Arizona.

**Figure 2.8** Lehmann Lovegrass.ScientificName:*Eragrostis Lehmanniana*.
Image from AtlanticMulch.com

Cheat Grass (*Bromus tectorum*) is an invasive plant introduced into the United States from central Asia (Figure 2.10). It has flat and narrow leaf blades that are around 2 mm– 3.5 mm broad and reaches a plant height of 2.5 cm – 50 cm (CABI., 2017). Cheatgrass germinates in abundance and is continuously covering lands across the United States. During fire seasons (summer), cheatgrass usually dies off and increases fire frequency due to its very fine and dry fuel characteristics (Zouhar, 2003). Cheatgrass often fuels wildfires that burn at much higher intensities and spread at a faster rate. (Simonin, 2001). Cheatgrass was collected during a hot summer day near the Box Springs mountains located nearby the University of California Riverside. An effort was made to collect cheat grass in locations where there clearly was no cross contamination from other grasses.

**Figure 2.9** Cheat grass. Scientific Name: *Bromus Tectorum*. Image from Winlawn.com

Wild oats (*Avena Fatua*) is an invasive species that originated from Asia (Figure 2.11). It reaches heights up to about 4 feet and is mainly used as livestock for cattle and horses. It is an "erect, cool-season annual grass with open-branches, nodding flower cluster" (UCIPM, 2016). It is a fine fuel that usually grows in in a cluster of small but feathery flower heads. Wild oats were collected near the Box Springs mountains by University of California, Riverside.
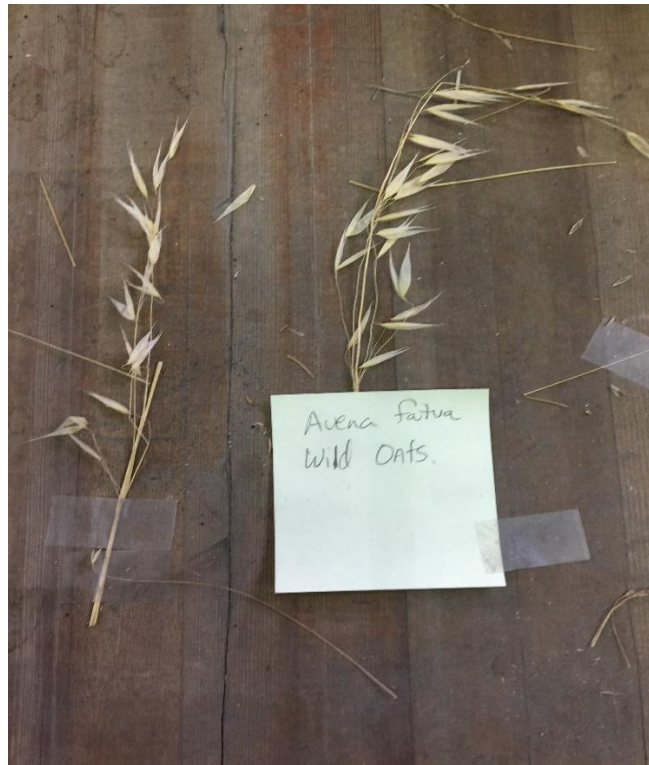
**Figure 2.10** Wild Oats. Scientific Name: *Aveena Fatua*

Timothy grass (*Phleum Pratense*) is a short-lived, cool-season perennial grass that grows up to 40 inches in height (Figure 2.12). The seed heads are tan with a fuzzy appearance. (Idaho Plant Materials Program, n.d.). Timothy grass is often used as livestock for horses and hamster food. Timothy grass was store bought, and initial interest arose when the fuzzy seed heads managed to smolder during preliminary testing.

**Figure 2.11** Timothy Hay. Scientific Name: *Phleum Pratense*

# 3.0 Background of Relevant Processes

This section provides insight into grinding with sufficient details given on involving processes and the main mechanistic analysis.

## 3.1 Grinding Processes

According to Jain (2009), kinetic energy is defined as the energy an object possesses due to its motion. The Law of Conservation of Energy states that energy cannot be created nor destroyed, but energy can only be transferred or changed from one form to another. During the grinding of a material, kinetic energy is transferred from the rotating disk to the point of contact mainly as heat. At this stage of the grinding, the grinding wheel is essentially abrading the metal to a temperature high enough to melt it. A large amount of this energy goes into the deformation/separation of the material, which has a strong influence on the initial temperature of the particle. The material's strength and ductility determine how much energy is required to deform/separate the material. The combination of strength and ductility equates to the material's toughness presented in Figure 3.1 which is "the ability of a metal to deform plastically and to absorb energy in the process before fracture" (NDT Education Research Center, n.d.). Unlike a material with low toughness, a tougher material will require a higher amount of deformation energy before fracturing. Therefore, the amount of energy per unit volume that a material can absorb before fracture may be measured by calculating the area under the stress-strain curve (Figure 3.2).
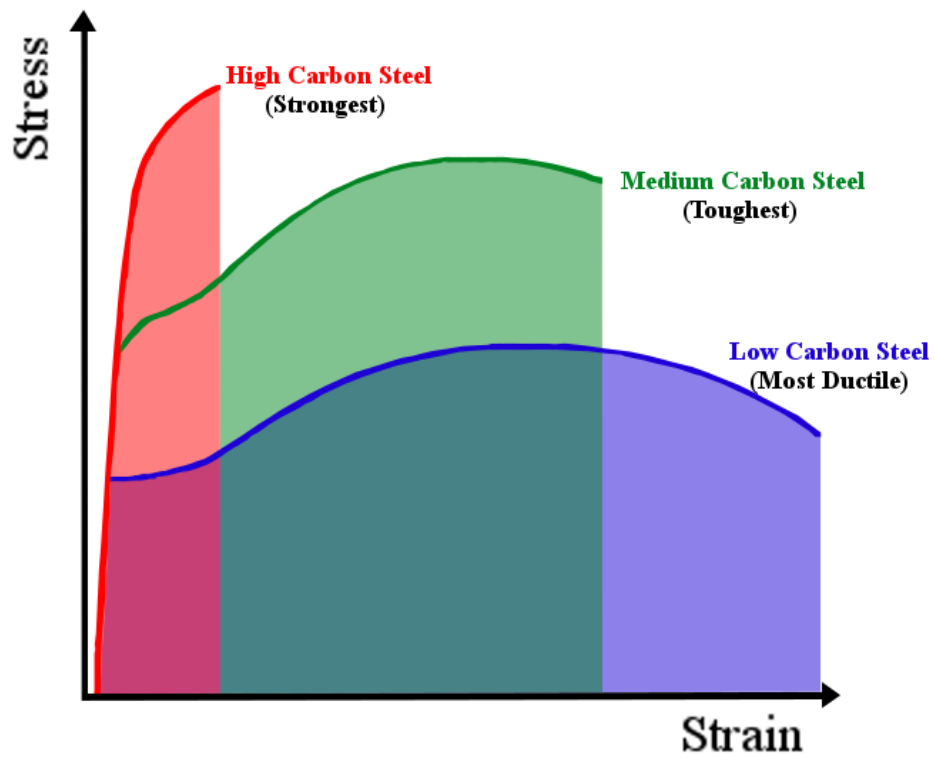
**Figure 3.1** Toughness Plot: Comparison of Different Percentages of Carbon. Comparison of how area under the curves changes for ductility vs strength but experiences an increase in area when combined to make a tougher material (Adopted from NDT Education Resource Center, n.d.)
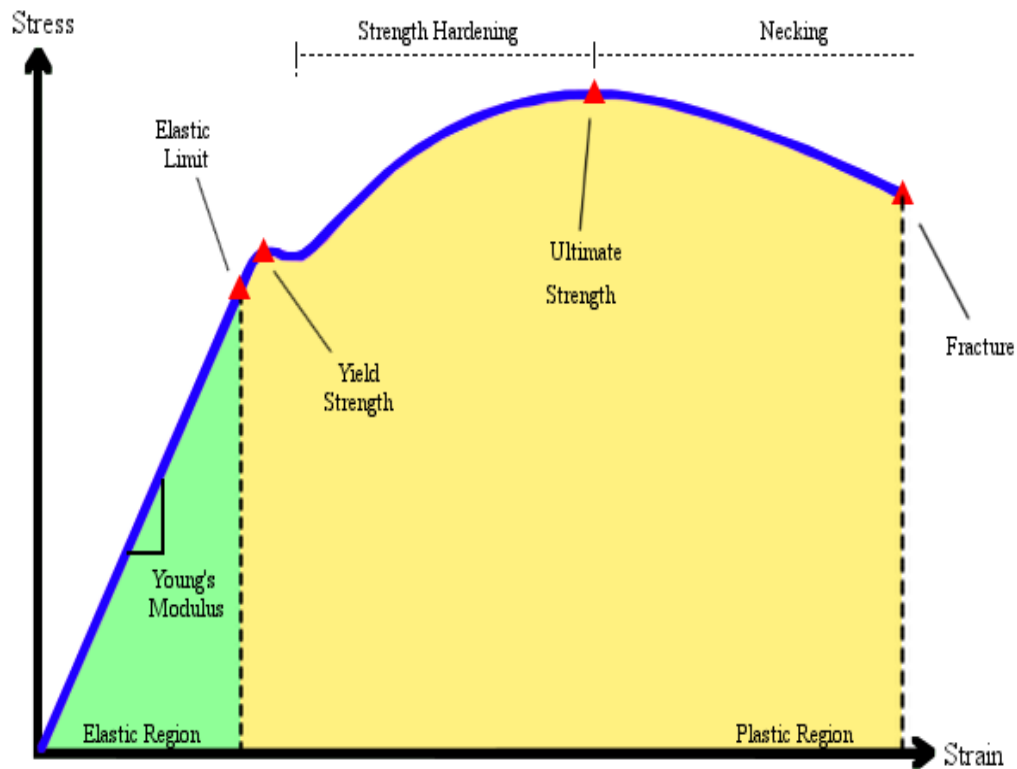
**Figure 3.2** Stress vs Strain Plot. Area under the stress-strain curve represents the amount of energy per unit volume that a material can absorb before fracture.

According to Behrend and Ritter (2004), a "higher strength material will result in smaller particles with higher initial temperatures, at which the melting temperature of the material can be reached as a maximum." They state that "with decreasing strength and ductility the material can more easily be deformed, and larger particles are created. At a high temperature of the grinding spot, accompanied by a low separation energy, the initial temperature of the particles corresponds to that of the grinding spot". From this, we can predict that cold rolled steel and stainless steel will generate smaller particles than copper due to the differences in toughness. The higher material toughness found in cold rolled

steel and stainless steel allows smaller pieces to be broken off due to the material's ability to fracture. Copper, a more ductile material, will generate larger particles due to the material's tendency to bend instead of fracture into small pieces. Tables 3.1 and 3.2 can be seen below which list the metals mechanical and thermal properties.

**Table 3.1** Mechanical Properties

| Material | Material Grade Selection | Yield Tensile Strength | Ultimate Tensile Strength | Brinell Hardness | Carbon Percentage |
|---|---|---|---|---|---|
| Cold Rolled Steel | AISI 1018 Steel, Cold Drawn | 370 MPa | 440 Mpa | 126 | 0.14 – 0.20 % |
| Stainless Steel | 304 Stainless Steel | 215 Mpa | 505 Mpa | 123 | ≤ .08 % |
| Copper | Copper Bar Alloy 110 | 33.3 Mpa | 210 Mpa | 50 | — |

**Table 3.2** Thermal Properties

| Material | Material Grade Selection | Specific Heat Capacity | Thermal Conductivity | Melting Point |
|---|---|---|---|---|
| Cold Rolled Steel | AISI 1018 Steel, Cold Drawn | $0.486\ \frac{J}{g\ ℃}$ | $51.9\ \frac{w}{m\ K}$ | 1400 – 1455℃ |
| Stainless Steel | 304 Stainless Steel | $0.500\ \frac{J}{g\ ℃}$ | $21.5\ \frac{w}{m\ K}$ | 1400 – 1455℃ |
| Copper | Copper Bar Alloy 110 | $0.385\ \frac{J}{g\ ℃}$ | $385\ \frac{w}{m\ K}$ | 1083 ℃ |

In addition to the deformation of the metal; which is a high energy process and greatly influences the starting temperature of the particle, the metal chip may further be heated by the oxidation process. Oxidation occurs as soon as the particle is exposed to the air which begins a chemical reaction. Nikiforov *et al.* (2017) investigated the combustion of a metal chip after grinding and found that "if the surface temperature of the chip exceeds the melting temperature of the oxide film" then combustion/burning occurs. An oxide film forms on the surface of the metal due to the metals exposure to oxygen. Figure 3.3 illustrates an algorithm created by Nikiforov *et al.* (2017) to determine the final form of the metal chip.
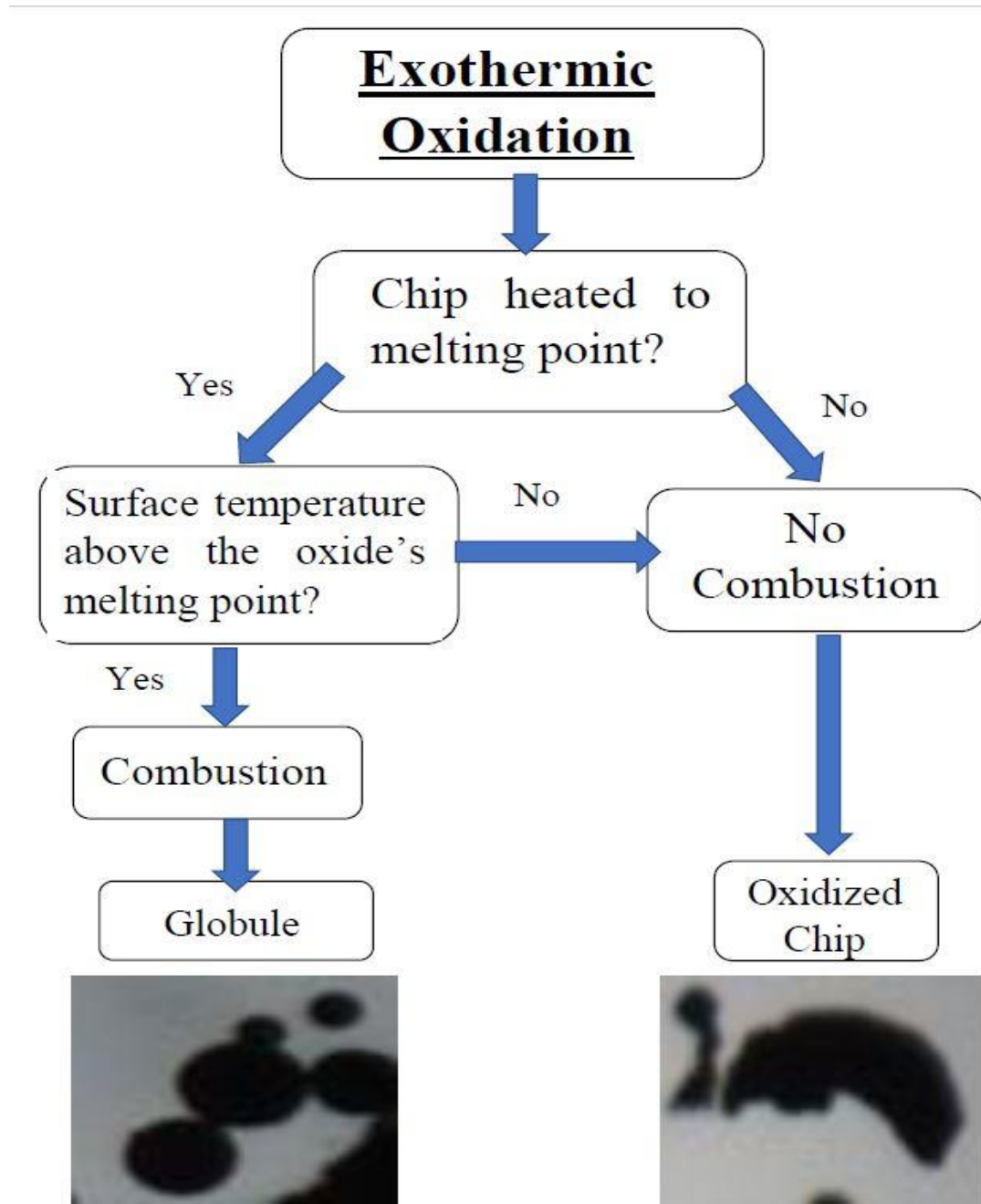
**Figure 3.3** Algorithm (adopted from Nikiforov *et al.*, 2017) for Determining Final Form of Metal Chip. Where globules are the cooling spherical metal droplets produced during the spark production from a metal, and metals chips are produced due to the lack of combustion of the metal particle.

The combustion of a metal chip is highly influenced by the following: the initial temperature of the chips (1), the nature of its heat exchange with the environment (2), the diffusion-oxidation processes (3), the strength characteristics of the outer layer and the value of the activation energy (4) (Lu et. al., 1992). In addition to these important factors, the size of the particle highly influences the temperature of the ejected metal chips. As stated before, a material with a greater toughness generates smaller size particles with a higher initial temperature and vice versa, for a material with lower toughness. The smaller chips are easier to ignite since they have a greater surface area on which to burn; therefore, increasing the temperature of the small chip rapidly and helping it reach its melting point. With the accumulation of energy and the rapidly increasing temperature, the surface temperature of the metal chip is increased above the oxide's melting point and allowed to combust and further be heated. Nikiforov *et al.* (2017) state that "if combustion is complete, the final product will be cooling spherical oxide droplets. If combustion is incomplete, metal droplets surrounded by a thick oxide shell will persist". The aforementioned spherical droplets are referred to as globules by Nikiforov *et al.* (2017), who studied and analyzed how these globules relate to the creation of sparks. In summary, he found that these globules are formed from the combustion of the metal chips and supported this theory by finding that non-combustible metals like copper do not possess these globules.

Lastly, Nikiforov *et al.* (2015), states that the "volume of the sparks is directly dependent on the quantity of the burning metal and carbon dioxide. The more carbon in the alloy is, the higher the temperature of the chips, the more carbon dioxide, the more sparks". This can be seen in Figure 3.4 which compares the volume of the sparks for different

metals. The volume of the sparks is important as this relates to the contact area it makes with the ignitable fuel.
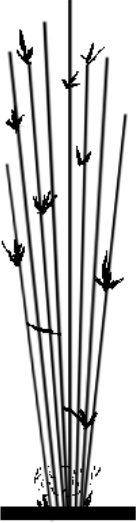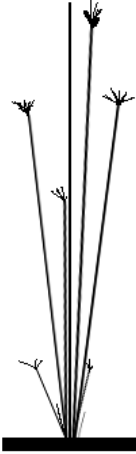


| Volume of Sparks for Metal Grinded | | | |
|---|---|---|---|
| High Carbon (C.R. Steel) Carbon Percentage: 0.14-0.20% | Low Carbon | Stainless Steel (S.S.) Carbon Percentage: ≤0.08% | Copper Carbon Percentage: None |

**Figure 3.4** Pictorial Representation (adapted from Nikiforov *et al.*, 2015) of Volume of Sparks for Different Metals

In summary (Refer to Figure 3.5),

1.) Metal particles/chips are very hot; having been deformed off a workpiece which is a high energy process

2.) Metals with a high toughness generate smaller metal chips from grinding; hence, have a high surface area on which to burn, but hardly any mass to carry heat away

3.) If the surface temperature of the chip exceeds the melting temperature of the oxide film, then combustion/burning occurs

4.) Metal particle will completely burn until completely oxidized, or oxygen can

no longer get to the surface of the material
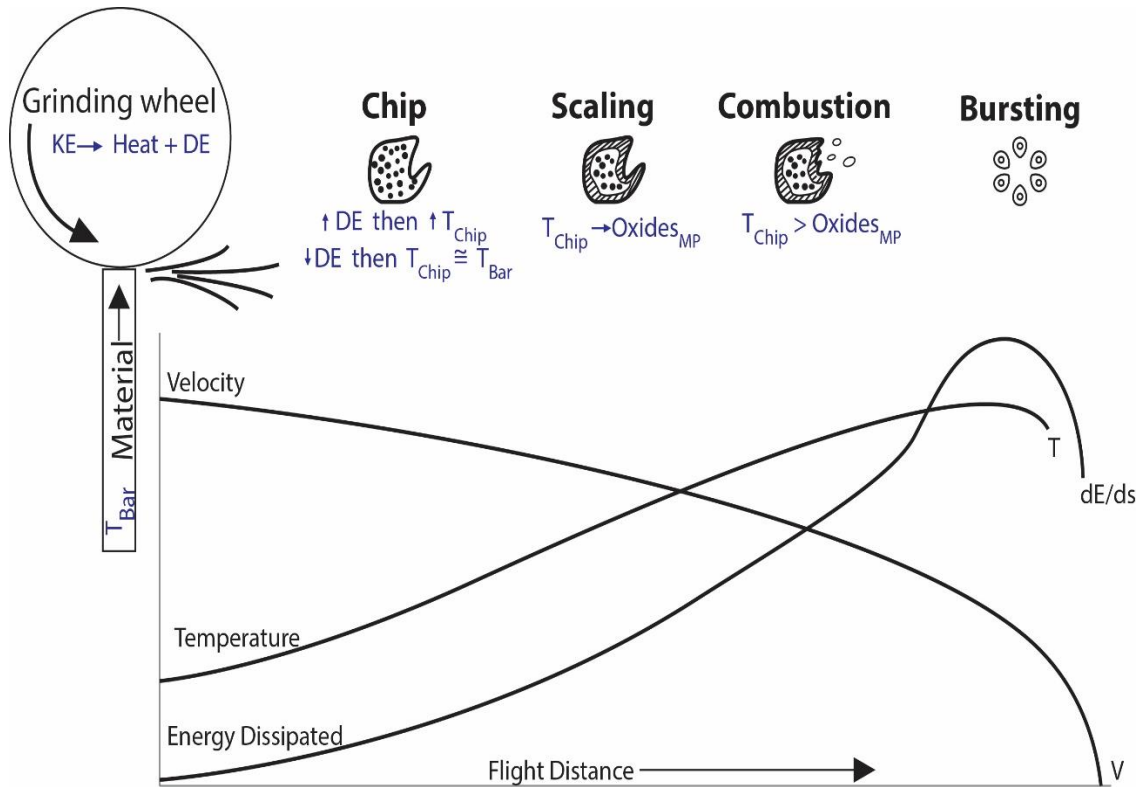


**Figure 3.5** Schematic of the Possible States of Sparks/Metal Chips Produced from Grinding. KE = Kinetic Energy produced from grinder; DE = Deformation energy produced to abrade metal; $T_{chip}$ = Temperature of metal chip produced from grinding; $T_{Bar}$= Temperature of the metal at the contact point between grinder and material; $Oxides\_mp$ = Oxides film melting point; T = Temperature, v = speed, De/ds = energy dissipated to the stationary environment per unit distance. Adopted from Behrend & Ritter (2004)

## 3.2 Heat Transfer Processes

This section gives the basics of relevant heat transfer processes. An analysis has been completed by Tse and Fernandez-Pello (1998) on the flight paths of metal particles and embers generated by power lines. Although the analysis focuses on particles generated by power lines, several subjects treated in his work are applicable to our research. Fernandez-Pello (1998) states "all particles, whether burning or not, obey the same laws for their trajectory paths."

After grinding, metal chips are expelled from the workpiece and travel a set distance before encountering the fuel. During flight, the expelled metal chips experience heat loss due to convection and radiation. Metal chips experience convection due to the particle falling through a fluid (air) and encountering a temperature difference between the particle and the fluid (air). Lumped capacitance is a special case of heat transfer that is applied to our case due to the particles being considered "thermally thin" (Incropera *et al.*, 2017). As presented by Tse and Fernandez-Pello and using lumped capacitance analysis, the temperature ( $T_P$ ) of a metal sphere particle is given by the following transient energy equation:

$$\rho V_p c_p \left( \frac{dT_P}{dt} \right) = \left( h A_p (T_P - T_\infty) + \sigma \varepsilon A_p (T_P^4 - T_\infty^4) \right) \qquad (1)$$

where $\rho, V, c$ are, respectively, the density ($kg/m^3$), volume ( $m^3$ ) and specific heat capacity ($J/(Kg\ K)$) of the metal particle; $\bar{h}$ is the convective heat transfer coefficient ( $W/m^2\ K$ ); $A_p$ is the surface area of the metal particle; $\sigma$ is the Stefan-Boltzman constant (5.67 x $10^{-8}\ W/m^2 K^4$ ) ; $\varepsilon$ is the emissivity of the particle, and $T_P\ and\ T_\infty$ are the initial

particle and ambient temperatures, respectively. The first and second terms on the right-hand side of equation 1 represent the heat losses due to convection and radiation, respectively. When the heat loss due to radiation is negligible as in cases like the ones here where the radiation heat transfer coefficient is approximately two orders magnitude less than the convection coefficient. Taking this into account, equation 1 becomes the following:

$$\frac{dT_P}{dt} = -\frac{1}{(\rho Vc)_P}\left(hA_p(T_P - T_\infty)\right) \tag{2}$$

Following the derivation presented in Incropera *et al.* 2017, equation 2 is rearranged and becomes:

$$-hA_S(T - T_\infty) = \rho Vc\frac{dT}{dt} \tag{3}$$

Substituting,

$$\theta \equiv T - T_\infty \tag{4}$$

If $T_\infty$ is constant and $\left(d\theta/dt\right) = \left(dT/dt\right)$, then equation 3 becomes:

$$\frac{\rho Vc}{hA_s}\frac{d\theta}{dt} = -\theta \tag{5}$$

Using separation of variables and integrating,

$$\frac{\rho Vc}{hA_S}\int_{\theta_i}^{\theta}\frac{d\theta}{dt} = -\int_0^t dt \tag{6}$$

Where $\theta_i \equiv T_i - T_\infty$ then,

$$\frac{\theta}{\theta_i} = \frac{T_f - T_\infty}{T_i - T_\infty} = exp\left[-\left(\frac{hA_s}{\rho Vc}\right)t\right] \tag{7}$$

where $T_f, T_i, and\ T_\infty$ are the final, initial and ambient temperatures. This allows us to solve

for the final temperature $(T_f)$ right before impact with the fuel.

The average heat transfer coefficient ($\overline{h}$) is determined from the average Nusselt number

($\overline{Nu}$), which represents the ratio of convective to conductive heat transfer across the

boundary.

$$\overline{Nu} = \frac{\overline{h}d_p}{k_{air}} \tag{8}$$

where k is the thermal conductivity of the surrounding fluid (air) ($W/(m * K)$) and $d_p$ is

the diameter of the particle (m) which represents the length scale of the object.

Fernandez Pello applied the correlation of Ranz and Marshall to find the average Nusselt

number for a spherical particle experiencing convective heat transfer:

$$\overline{Nu} = 2 + 0.6Re^{1/2}Pr^{1/3} \tag{9}$$

where $Re$ is the Reynolds number which is a dimensionless value that measures the ratio

of inertial forces to viscous forces in the flow and describes if the flow is laminar or

turbulent. $Pr$ is the Prandtl number, a dimensionless number approximating the ratio of momentum diffusivity to thermal diffusivity.

The Prandtl number ($Pr$) is given as:

$$Pr = \frac{c_p \mu}{k} \tag{10}$$

where $c_p$ is the specific heat of the particle $J/(kg * K)$, $\mu$ is the dynamic viscosity of the fluid (air) $(N * s)/m^2$ and k is the thermal conductivity $W/(m * K)$.

The Reynolds number ($Re$) may be expressed as the following:

$$Re = \frac{\overline{U} d_p}{v_{air}} \tag{11}$$

where $\overline{U}$ is the velocity of the fluid with respect to the particle $(m/s)$, $d_p$ is the diameter of the particle (m) which represents the characteristic length of the object (m), and $v_{air}$ is the kinematic viscosity of the fluid (air) $(m^2/s)$.

Determining the Reynolds number requires the ejected metal chip (particle) velocity to be identified. The velocity is difficult to quantify due to the small-scale size of the metal chips. It was assumed that metal chips velocity was approximately equal to the rotational velocity of the grinder. For example, assuming the grinder rotates at a constant 10,000 RPM with a grinder wheel diameter of 4.5 inches then multiplying together will give us a rotational velocity of 59.84 m/s.

# 4.0 Laboratory Results and Discussions

This section describes the observations made from the experimental results.

## 4.1 Classification of Experiments

The experiments were classified into three major groups- simply, Set 1, Set 2, and Set 3, as summarized in Figure 4.1. Each consisted of subgroups (classes) for thorough analysis and presentation of the results. Set 1 consisted of the following classes: SS, CR, Cu. Set 2 consisted of SS/CR-Wo, SS/CR-Cg, and SS/CR-Th. Finally, Set 3 consisted of CR-Cg. A detailed description of each set of experiments is given next.
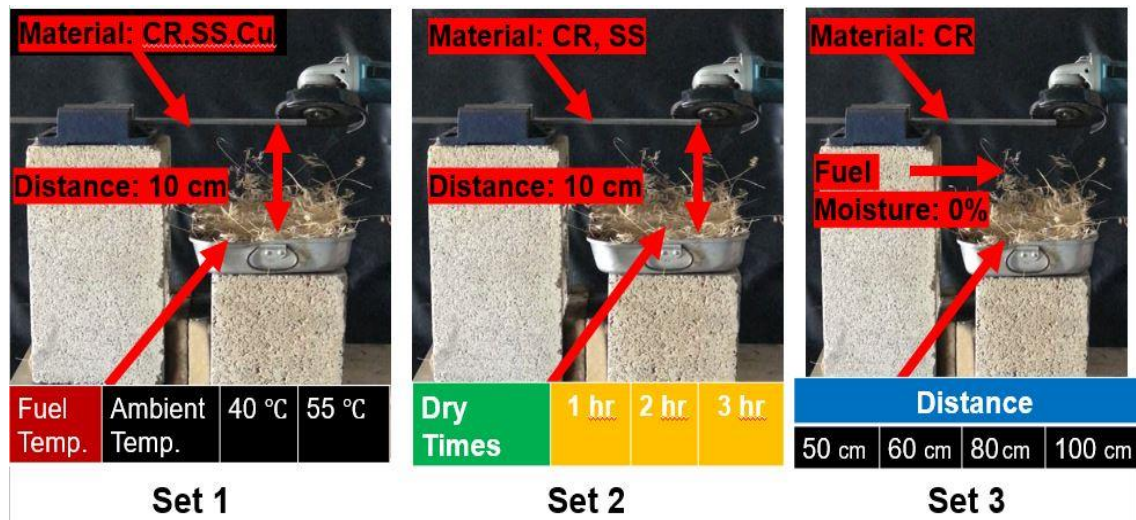


**Figure 4.1** Summary of Classification for all Sets

### 4.1.1 Description of Set 1 Experiments (Classes: SS, CR, Cu)

For the first set of experiments, the following three parameters were controlled: the fuel material (FM), bar material (BM), and temperature of the fuel (Table 4.1).

**Table 4.1** Classification of Experiments for Set 1. Each material and fuel combination is tested for three fuel temperatures: ambient, 40$^o$C, and 60$^o$C

| Classification | Material & Fuel Type | Fuel Temp. | Ambient Temperature | 40 Celsius | 55 Celsius |
|---|---|---|---|---|---|
| **SS** | Stainless Steel | Lovegrass | ✔ | ✔ | ✔ |
| | | Timothy | ✔ | ✔ | ✔ |
| | | Wildoats | ✔ | ✔ | ✔ |
| **CR** | Cold Rolled Steel | Lovegrass | ✔ | ✔ | ✔ |
| | | Timothy | ✔ | ✔ | ✔ |
| | | Wildoats | ✔ | ✔ | ✔ |
| **Cu** | Copper | Lovegrass | ✔ | ✔ | ✔ |
| | | Timothy | ✔ | ✔ | ✔ |
| | | Wildoats | ✔ | ✔ | ✔ |

Prior research has already shown that inert fuel characteristics, like fuel moisture, are significant when determining ignition probability of a fuel. However, the three parameters (FM, BM, and the temperature of fuel) listed above provided a more simplistic approach to the understanding of our work. Different bar materials were chosen because this varied the material's mechanical and thermal properties. Stainless steel, cold rolled steel, and copper were the three selected bar materials. Copper was chosen because it can

be found in clashing conductors, which has been shown to possess the probability of starting ignition of wildland fuels (Tse and Fernandez-Pello, 1998). Alternatively, aluminum, also found in clashing conductors, was considered. However, as prior research shows, aluminum does not produce sparks during grinding processes, so was not a primary focus of our study. Stainless steel and cold rolled were chosen because they are common materials used when machining and grinding.

The fuel temperatures were varied by placing the fuel in an oven and allowing it to reach a steady temperature of either 40 °C or 55 °C, varying between experiments. The temperature of 40 °C was chosen to match that of an average summer day, and 55 °C was selected to replicate that of the higher extremes of the summer months. The fuel at ambient temperature for that day was chosen for comparison to moderate conditions which, at the time of experiments, typically ranged from 25 °C to 30 °C. A total of three trials were repeated for each respective combination listed in the matrix above (Table 4.1), resulting in a total of 81 experiments. Table A.1 may be found in Appendix A, which summarizes the measured parameters of each experiment that include the following: the experiment number, time of day, ambient temperature, relative humidity, fuel distance, the mass of fuel and measured dead fuel moisture. Hence, the classification of the first set of experiments was separated into three classes- SS, CR, and Cu-as summarized in Table 4.1. The purpose of set 1 was to find the best combinations (metal, fuel type, and fuel temp.) which possessed the highest ignition probabilities based on the experiments.

## 4.1.2 Description of Set 2 Experiments (Classes: SS/CR-Wo, SS/CR-Cg, SS/CR-Th)

For the second set of experiments, the metal, fuel type and fuel moisture were varied to find the effect they have on ignition. Copper was eliminated in the second set of experiments since it only caused ignition in two out of the 27 previous trials. Copper did produce smoldering ignition in most experiments, but it was decided to focus on the materials that caused flaming ignition which was the more extreme condition.

The main difference between the second set and first set of experiments is that fuel moisture was altered significantly for the second set. In the first set of experiments, the fuel moisture varied with the fuel temperature and was typically low (*i.e.*, 2%-6%) since the fuels were heated; thus, lowering the fuel moisture. The purpose of the second set of experiments was to observe how the same metal particles (sparks) interacted with fuel beds of higher fuel moisture (20% - 80%). This process would help us identify which of these two metals possessed the highest ignition capability when encountering higher fuel moistures. Attempts were made to accurately control the fuel moisture by using a humidifier, but this process was dismissed in favor of a much simpler and time-efficient approach. The following was the alternative process that we chose to follow. The fuel moisture was varied by soaking the fuels in a water tank for a total of five minutes and allowing it to air dry for different increments of time: 1 hour, 2 hours, or 3 hours. At the desired hour, three fuel samples were collected in plastic bottles, and the gross wet weight was recorded before placing it in the oven. Once removed from the oven, the bottle cap

was immediately placed on the bottle sample and allowed to cool down before measuring the gross dry weight. Hence, the fuel moisture was calculated as:

$$Fuel\ Moisture = \frac{Net\ Wet\ Weight - Net\ Dry\ Weight}{Net\ Dry\ Weight} \qquad (12)$$

where the net wet weight is total wet weight (wet fuel weight plus bottle weight) subtracted by the weight of the bottle, and the net dry weight is total dry weight subtracted by the weight of the bottle.

A total of three replications were repeated for each respective combination listed in the matrix below (Table 4.2), resulting in a total of 54 experiments. Hence, the classification of the second set of experiments was separated into three classes SS/CR-Wo, SS/CR-Cg, and SS/CR-Th. Table A.2 may be found in Appendix A, which summarizes the measured parameters of each experiment, which include the following: experiment number, time of day, ambient temperature, relative humidity, fuel distance, mass of fuel and measured dead fuel moisture.

**Table 4.2** Experimental Classification for Set 2

| Material | Dry Time | 1 hr | 2 hr | 3 hr | Classification |
|---|---|:---:|:---:|:---:|:---:|
| Stainless Steel | Wildoats | ✓ | ✓ | ✓ | **SS-Wo** |
| | Cheatgrass | ✓ | ✓ | ✓ | **SS-Cg** |
| | Timothy Hay | ✓ | ✓ | ✓ | **SS-Th** |
| Cold Rolled Steel | Wildoats | ✓ | ✓ | ✓ | **CR-Wo** |
| | Cheatgrass | ✓ | ✓ | ✓ | **CR-Cg** |
| | Timothy Hay | ✓ | ✓ | ✓ | **CR-Th** |

### 4.1.3 Description of Set 3 Experiments (Class: CR-Cg)

For the third set of experiments, the interaction between the mechanically generated sparks and the fuel bed was investigated by varying the distance from the fuel bed to the grinder (cutting zone). This set of experiments was designed to model real-life applications such as a user standing when grinding a metal workpiece. The previous sets were performed to gain a basic understanding of which combinations possessed the highest ignition probability and how varying the fuel moisture further affected this probability. These previous sets, in turn, lead us to eliminate the metals and fuels with the lowest ignition capabilities. Cold rolled steel proved to possess the highest ignition capability of all three metals. For third set of experiments, the fuel was oven dried so, by definition, the fuel moisture was theoretically 0%. This was done to ensure that fuel moisture did not play a critical role in determining ignition, but rather how the varying distance affected the ignition probability. A total of 23 experiments was run for Set 3. Of those 23 experiments, eight were run at a distance of 100 cm, six were run at distances of 80 cm and 60 cm, and three were run at a distance of 50 cm. Consequently, the classification of the third set consisted of one class (CR-Cg) as summarized in Table 4.3. Table A.3 may be found in Appendix A, which summarizes the measured parameters of each experiment which include the following: experiment number, time of day, ambient temperature, relative humidity, fuel distance, mass of fuel and measured dead fuel moisture.

**Table 4.3** Experimental Classification for Set 3

| Fuel Distance / Material & Fuel Type | | 50 cm | 60 cm | 80 cm | 100 cm | Classification |
|---|---|---|---|---|---|---|
| Cold Rolled Steel | Cheatgrass | ✔ | ✔ | ✔ | ✔ | CR-Cg |
| | | ✔ | ✔ | ✔ | ✔ | |
| | | ✔ | ✔ | ✔ | ✔ | |

# 4.2 Results of Set 1 Experiments – Varying Fuel Temperature Experiments

## 4.2.1 Class CR

The experiments under Class CR focused on the combination(s) of cold rolled steel with each fuel at the three individual fuel temperatures (*i.e*., ambient temp., 40 °C, 55 °C). The distance from the fuel bed to the grinder was set at 10 cm for all experiments under set #1. From Figure 4.2., we can see that most of the experiments (19 out of 27) ignited under 50 seconds within a fuel moisture range from 2% to 6%. The transition from smoldering to flaming was highly observed for timothy fuel. From Figure 4.2, timothy mostly ignited when the fuel moisture was in the range of 2% to 4%, varying greatly from the other fuels that typically ignited with fuel moistures above 4%. Along with the observations made in

Class CR, SS, and Cu, we were able to deduce that timothy grass had the lowest ignition probability amongst all three fuels. However, it continued being used in set 2 of experiments for further study. Preliminary experiments started around November and ended January, which is considered to be during the winter. Hence, ambient temperatures were recorded to be around 21 ℃, a notable difference compared to our later experiments when the ambient temperature was around 30 ℃. This can be seen in Figure 4.3, where we were dealing with temperatures as low as 25 ℃ at the start of our experiments. These observations led us to the postulate that 29 ℃ was a critical temperature and that anything above that temperature would increase the ignition probability for that day. This can be supported by the cluster of ignitions seen above

 29 ℃ in Figure 4.3.
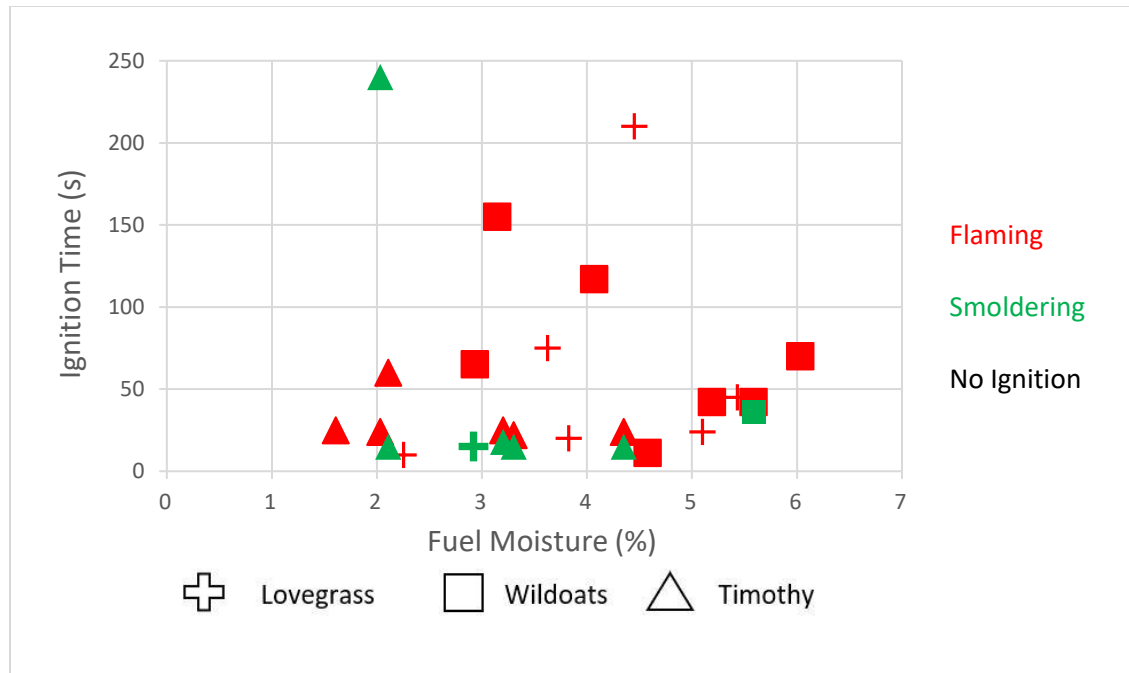
**Figure 4.2** Fuel Moisture vs. Time for Class CR. Fuel moisture vs. ignition time for all fuels (respective shapes) in combination with Cold Rolled Steel. Showing flaming ignition (red), smoldering ignition (green) and no ignition (black).
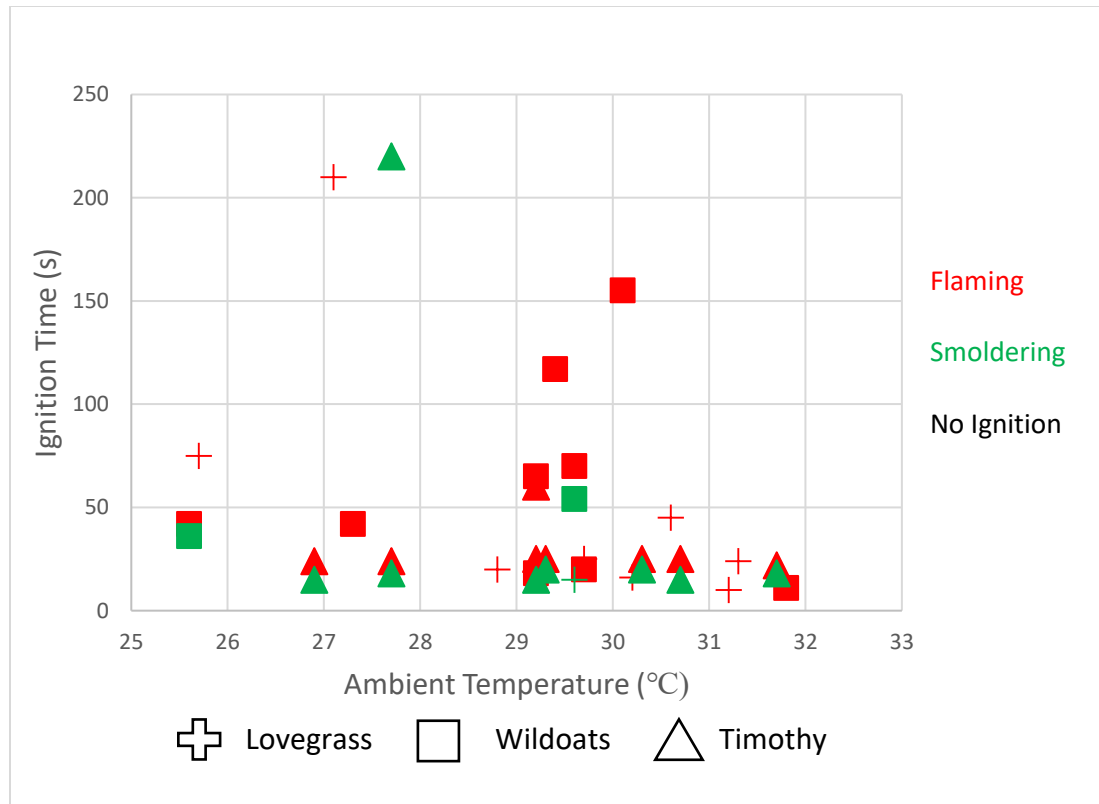
**Figure 4.3** Ambient Temperature vs. Ignition Time for Class CR. Ambient temperature vs. ignition time for all fuels (respective shapes) in combination with Cold Rolled Steel. Showing flaming ignition (red), smoldering ignition (green) and no ignition (black).

### 4.2.2  Class SS

The experiments under Class SS analyzed how stainless steel interacted with each fuel at the respective temperatures. The main result from Class SS is similar to the result of Class CR; it possessed a higher ignition capability than that of copper. However, the time to ignition was much more scattered for Class SS when compared to Class CR, as can be seen from Figure 4.5. For Class CR, most experiments ignited under 50 seconds and were clustered for ambient temperatures above 29 °C (Figure 4.3). The discrepancy in time to ignition may be attributed to the difference in carbon percentages between stainless steel and cold rolled steel. As mentioned before, cold rolled steel produces a greater volume of sparks because it has a carbon percentage of about 0.14 % to 0.20%, much greater than that of stainless steel ($\leq$ 0.08%). This increase in volume increases the contact area that the sparks make with the fuel, which increases the chances of ignition and decreases the amount of time it takes to ignition. The difference in volume of sparks may be seen from the images obtained from the high-speed camera (Figure 4.6).
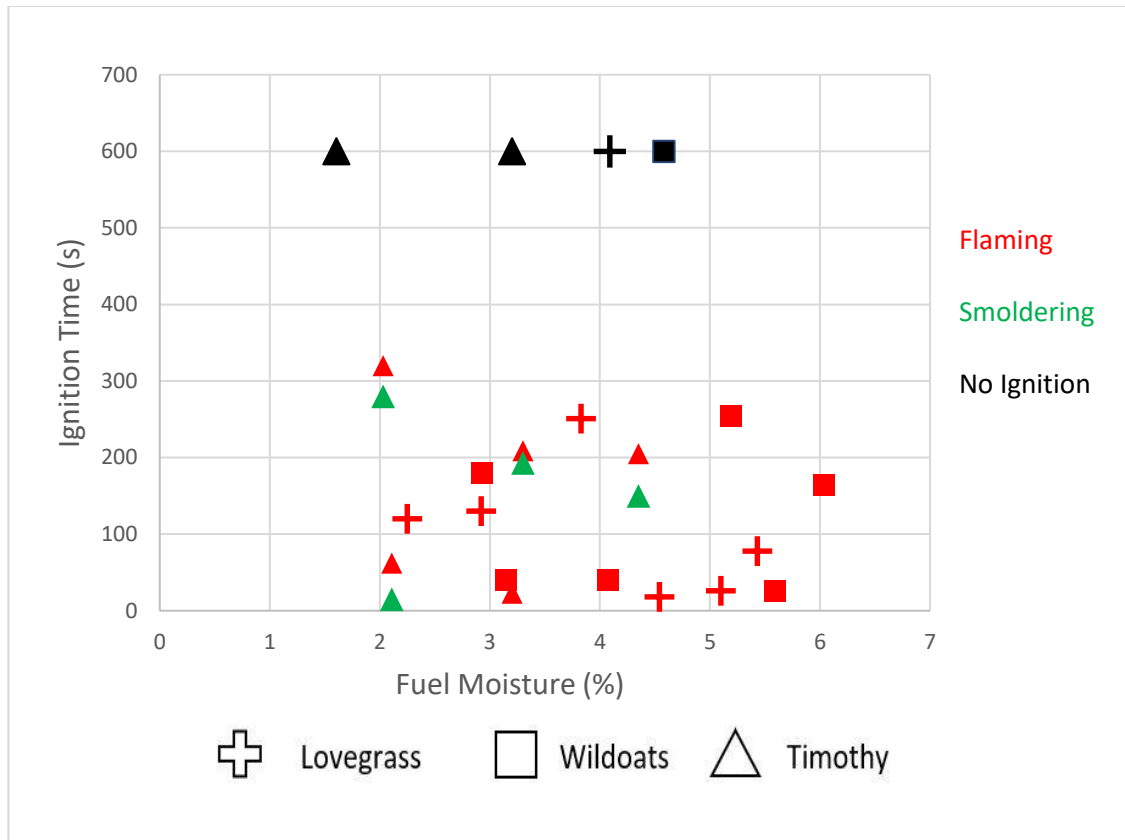
**Figure 4.4** Fuel Moisture vs. Ignition Time for Class SS. Fuel moisture vs. ignition time for all fuels (respective shapes) in combination with Stainless Steel. Showing flaming ignition (red), smoldering ignition (green) and no ignition (black).
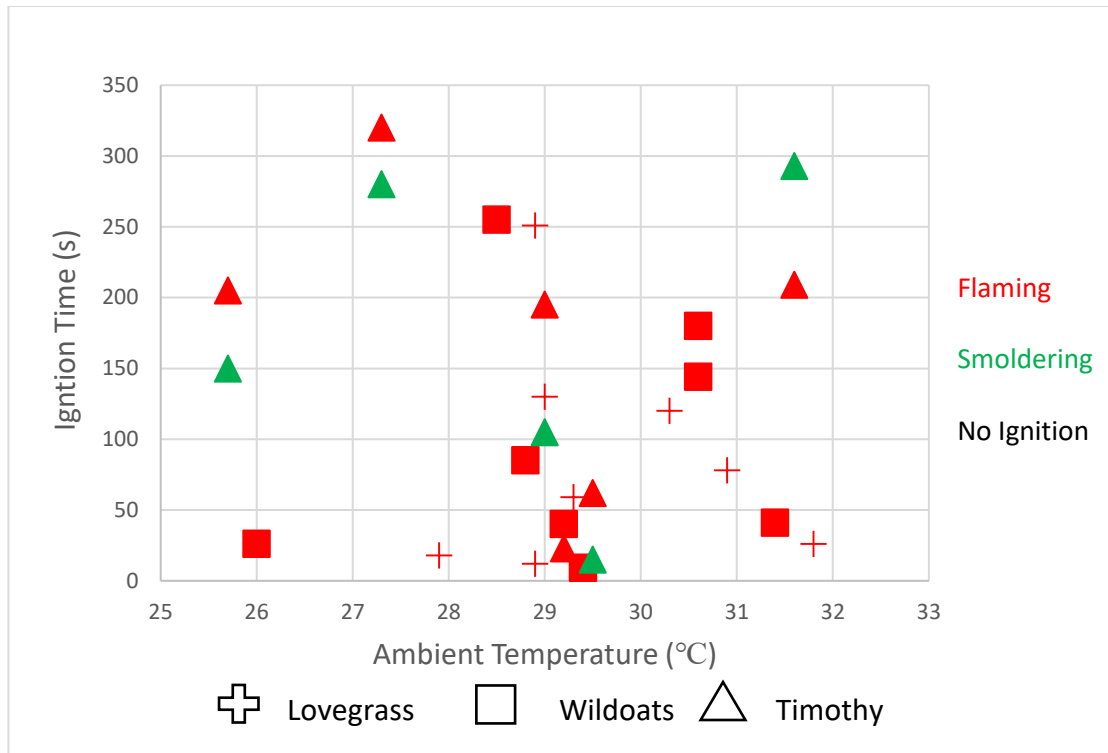
**Figure 4.5** Ambient Temperature vs. Ignition Time for Class SS. Ambient temperature vs. ignition time for all fuels (respective shapes) in combination with Stainless Steel. Showing flaming ignition (red), smoldering ignition (green) and no ignition (black).

**Cold Rolled Steel**          **Stainless Steel**

**Figure 4.6** Comparison of Volume of Sparks. Images acquired from the high-speed camera of difference in volume of sparks for cold rolled steel (left-hand side) and stainless steel (right-hand side).

### 4.2.3 Class Cu

The experiments under Class Cu were focused on the combination of copper with each fuel, at a respective temperature. Under Class Cu, only two out of 27 experiments flamed and 10 out of 27 experiments smoldered (Figure 4.8). The remainder of the fifteen experiments did not ignite after five minutes of grinding. This class was interesting as the diameter of copper particles ranged from 0.4375 to 2.5 mm and were larger than the stainless or cold rolled steel particles (0.0625 mm to 0.80 mm). The larger particles are expected to have a higher thermal mass and deliver a higher amount of energy to the fuel upon impact. However, the multiple cases with no ignition demonstrated otherwise. The multiple cases of smoldering imply that an insufficient amount of heat flux was provided in order for the fuel to transition to flaming. This can be attributed to the circumstance that copper does not combust because the initial temperatures of the copper particles/chips are

51

low due to the low separation energy. As a result, the copper particles were further impeded

from heating up and reaching a temperature above their oxide melting point.
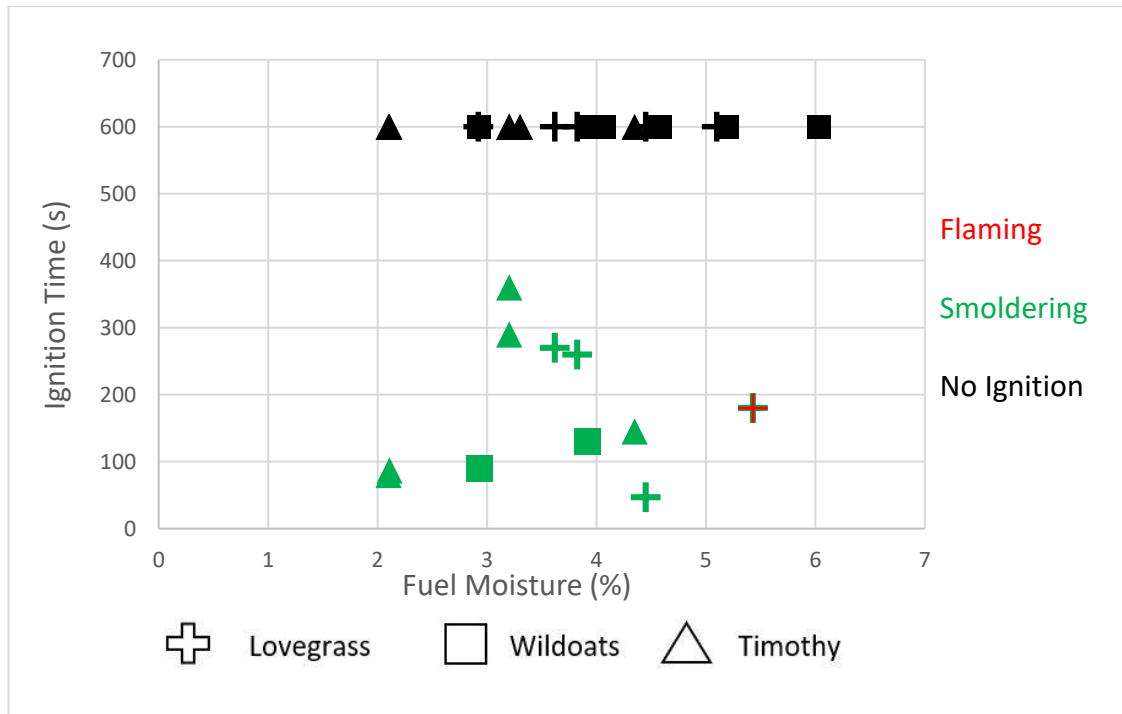


**Figure 4.7** Fuel Moisture vs. Time Copper. Fuel moisture vs. ignition time for all fuels (respective shapes) in combination with Copper. Showing flaming ignition (red), smoldering ignition (green) and no ignition (black).
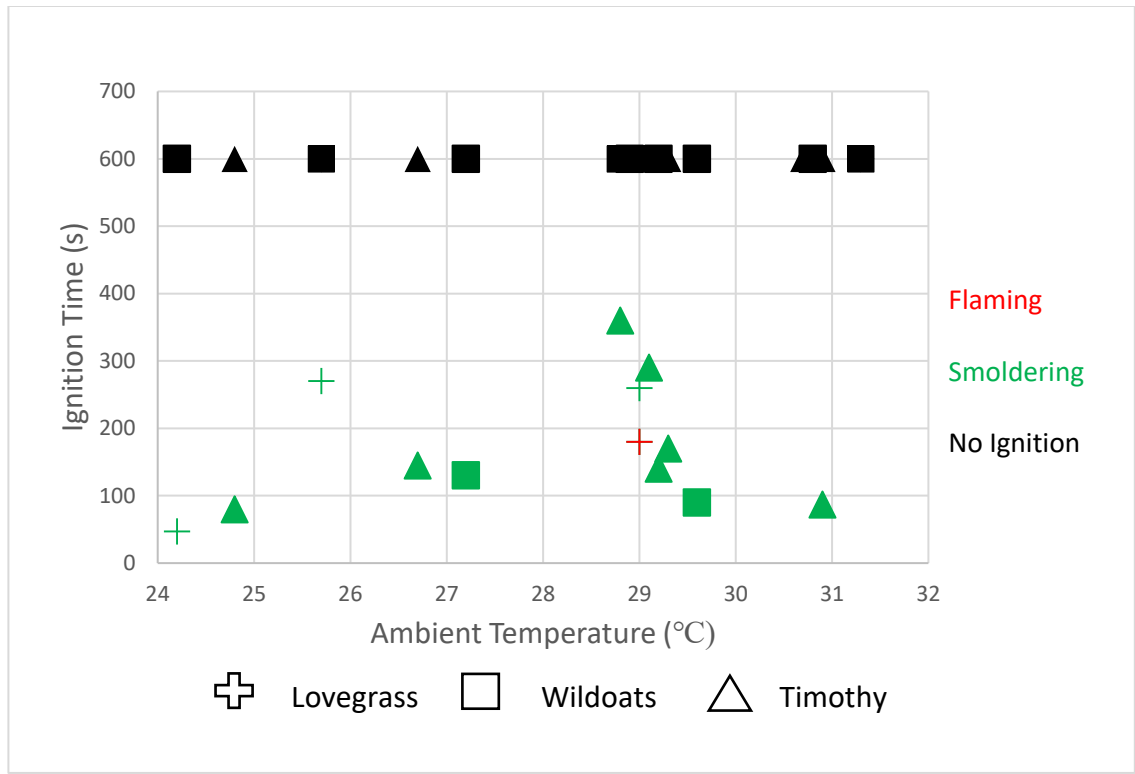
**Figure 4.8** Ambient Temperature vs. Ignition Time for Class Cu. Ambient temperature vs. ignition time for all fuels (respective shapes) in combination with Copper. Showing flaming ignition (red), smoldering ignition (green) and no ignition (black).

## 4.2.4  Statistical Analysis of Mean Ignition Times for Set 1

This section provides the calculated mean and standard deviation for each sample of set 1 using student's t-value distribution. Figure 4.9 list the mean ignition times with corresponding error bars. The error bars consist of the sample standard error multiplied by the t-value.



**Figure 4.9** Effect of Metallic Sparks on Mean Time to Ignition for Several Wildland Fuels. Error bars indicate the standard error multiplied by the respective t-value of the observed data.

## 4.3 Results of Set 2 Experiments - Varying Fuel Moisture Experiments

### 4.3.1 Class SS/CR-Wo

This subclass of experiments studied the interaction of stainless steel and cold rolled steel with varying wildoats fuel moistures. As previously stated, copper was eliminated, as it was found to have the least amount of direct flaming ignitions from set 1. From set 1, it was determined that stainless steel and cold rolled steel had the highest ignition capabilities and became the focus of our studies. Moreover, the main objective of set 2 was to study how the same metals would interact with significantly different ranges of fuel moistures. The initial hypothesis was that no fuel would flame nor smolder for fuel moistures above 30 %, considered to be the threshold of dry fuels (National Oceanic and Atmospheric Administration, n.d.). However, some of these experiments proved contradictory to this claim; four experiments smoldered or flamed at fuel moistures above 60 % (Figure 4.10). The following two observations of interest were made. First, most ignitions occurred with cold rolled steel, which is symbolized by the square shape. This was highly observed for all three fuels in combination with cold rolled steel; this helped us eliminate stainless steel and aimed our focus on cold rolled steel for set 3 of experiments. The second observation made was that the ambient temperature once again played a key role in determining whether the fuels would ignite. From Figure 4.11, we can see that most experiments with an ambient temperature above 29 ℃ ignited but any experiments under 29 ℃ rarely ignited. Specifically, eight experiments were conducted under 29 ℃, and 87 % of those experiments did not ignite (*i.e.*, seven out of eight experiments). However,

twelve experiments were conducted at an ambient temperature above 29 °C, and only 41% of those experiments did not ignite (*i.e*., five out of 12 experiments). This observed temperature threshold agreed with the same observed temperature threshold found in set 1 of experiments. Although flaming ignition was observed to be low (*i.e*., five out of 20 experiments) when compared to the previous set, the following two trends were observed; (1) the possible ambient temperature thresholds and (2) the most successful metal in igniting different fuels.
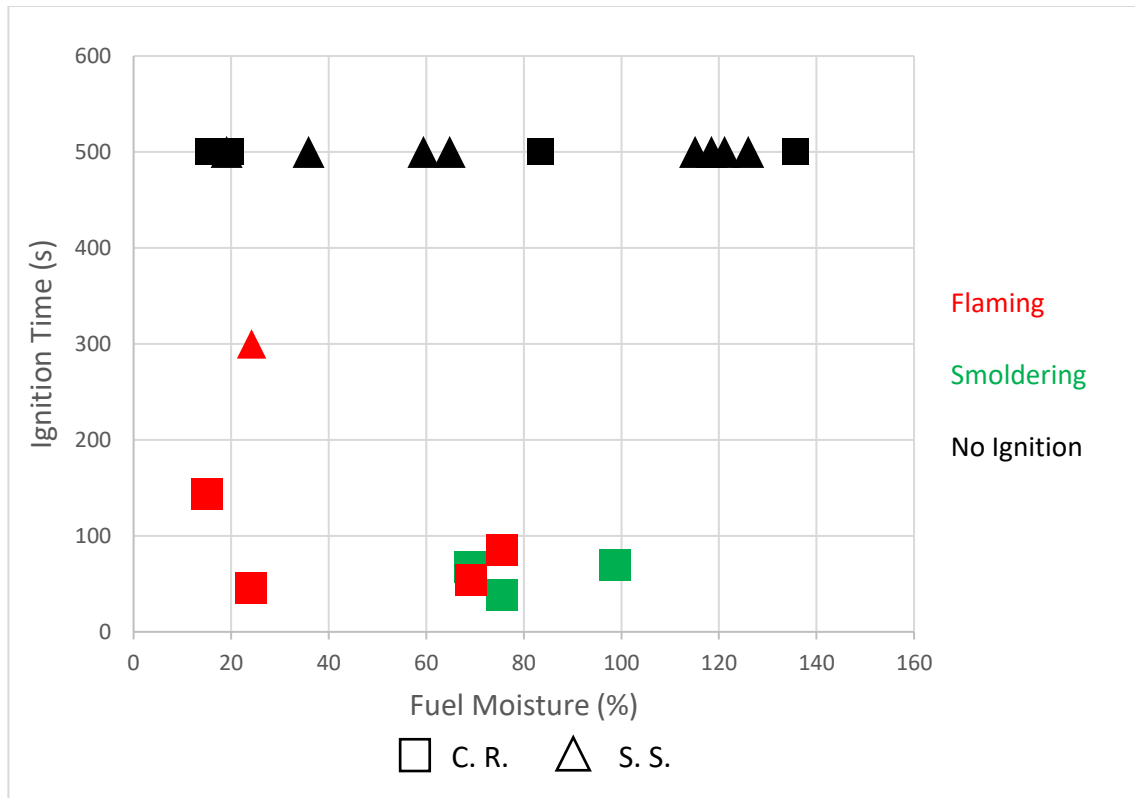
**Figure 4.10** Fuel Moisture vs. Ignition Time for Class SS/CR-Wo. Fuel moisture vs. ignition time for soaked Wildoats fuel in combination with Cold Rolled Steel (Square) and Stainless (Triangle). Showing flaming ignition (red), smoldering ignition (green) and no ignition (black). Corresponding dry times of 1 hour (smallest shape/icon), 2 hours (largest shape/icon), and 3 hours (median shape/icon).

**Figure 4.11** Ambient Temperature vs. Ignition Time for Class SS/CR-Wo. Ambient temperature vs. ignition time for soaked Wildoats fuel in combination with Cold Rolled Steel (Square) and Stainless (Triangle). Showing flaming ignition (red), smoldering ignition (green) and no ignition (black). Corresponding dry times of 1 hour (smallest shape/icon), 2 hours (largest shape/icon), and 3 hours (median shape/icon).

## 4.3.2  Statistical Analysis of Mean Ignition Times for Class SS/CR-Wo

This section provides the calculated mean and standard deviation for each sample of set 2 using student's t-value distribution. Figure 4.12 list the mean ignition times with corresponding error bars. The error bars consist of the sample standard error multiplied by the t-value.
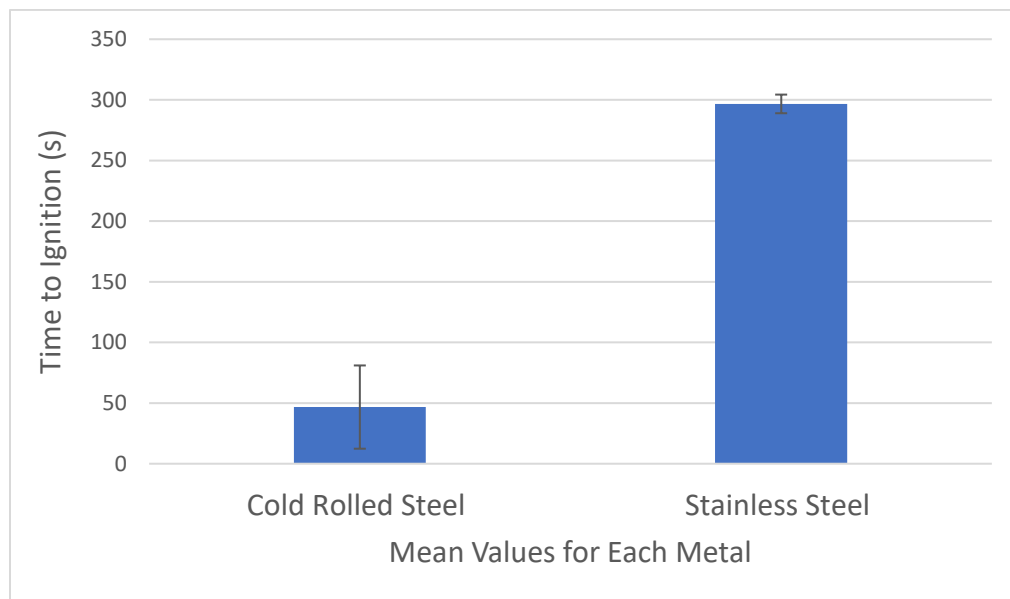


**Figure 4.12** Effects of Metallic Sparks on Mean Time to Ignition for Wildoats Fuel. Error bars indicate the standard error multiplied by the respective t-value of the observed data

## 4.3.3  Class SS/CR-Cg

This class of experiments studied the interaction of the previous two metals (*i.e.*, stainless steel and cold rolled steel) with Cheatgrass. As was the case in the previous class, it was observed that cold rolled steel dominated all the observed ignitions. However, the same ambient temperature threshold was applied but did not hold as strong for this fuel.

Four experiments were run at ambient temperature under 29 °C, and 75% of those experiments did not ignite (Figure 4.14). Although 14 experiments were conducted above 29 °C, 71% of those experiments did not ignite (10 out of 14).
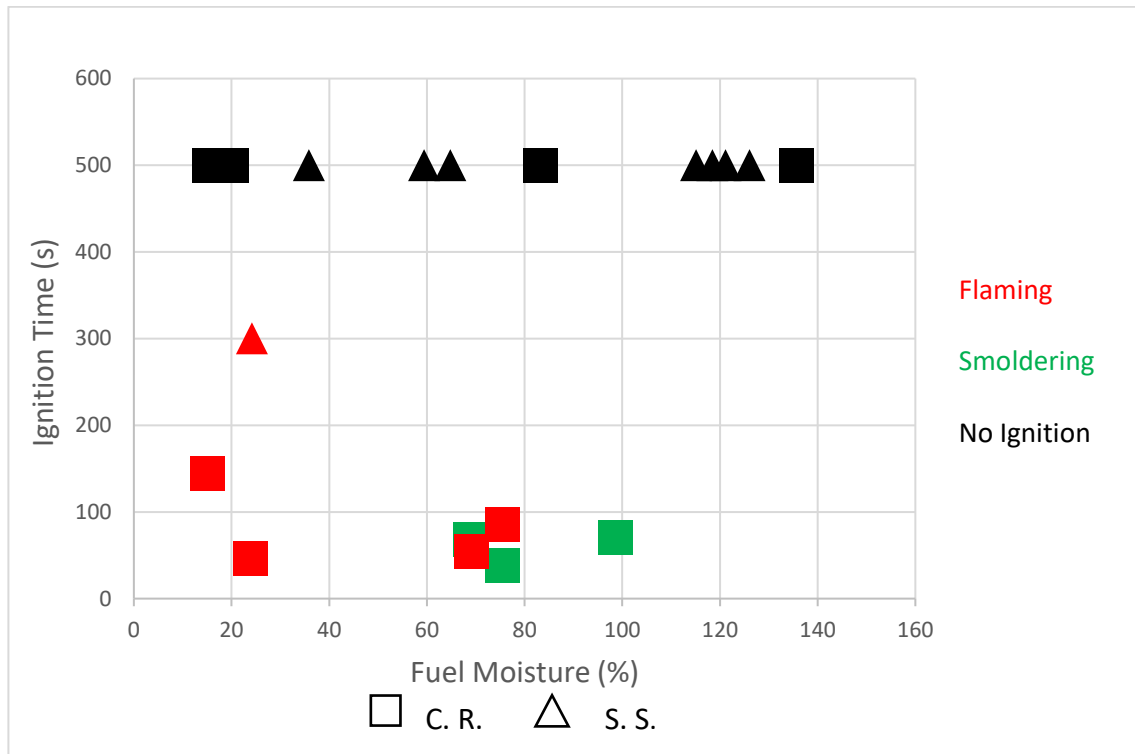


**Figure 4.13** Fuel Moisture vs. Ignition Time for Class SS/CR-Cg. Fuel moisture vs. ignition time for soaked Cheatgrass fuel in combination with Cold Rolled Steel (Square) and Stainless (Triangle). Showing flaming ignition (red), smoldering ignition (green) and no ignition (black). Corresponding dry times of 1 hour (smallest shape/icon), 2 hours (largest shape/icon), and 3 hours (median shape/icon).
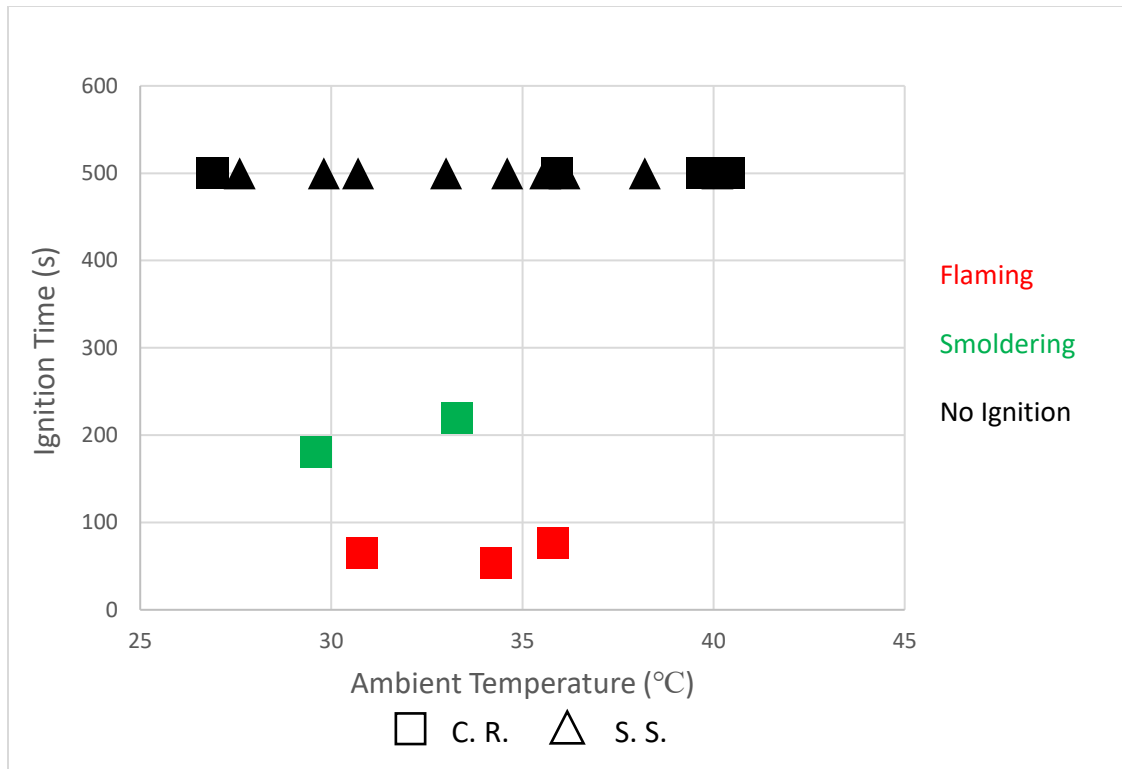
**Figure 4.14** Ambient Temperature vs. Ignition Time for Class SS/CR-Cg. Ambient temperature vs. ignition time for soaked Cheatgrass fuel in combination with Cold Rolled Steel (Square) and Stainless (Triangle). Showing flaming ignition (red), smoldering ignition (green) and no ignition (black). Corresponding dry times of 1 hour (smallest shape/icon), 2 hours (largest shape/icon), and 3 hours (median shape/icon).

### 4.3.4 Statistical Analysis of Mean Ignition Times for Class SS/CR-Cg

This section provides the calculated mean and standard deviation for each sample of set 2 using student's t-value distribution. Figure 4.15 list the mean ignition times with corresponding error bars. The error bars consist of the sample standard error multiplied by the t-value.
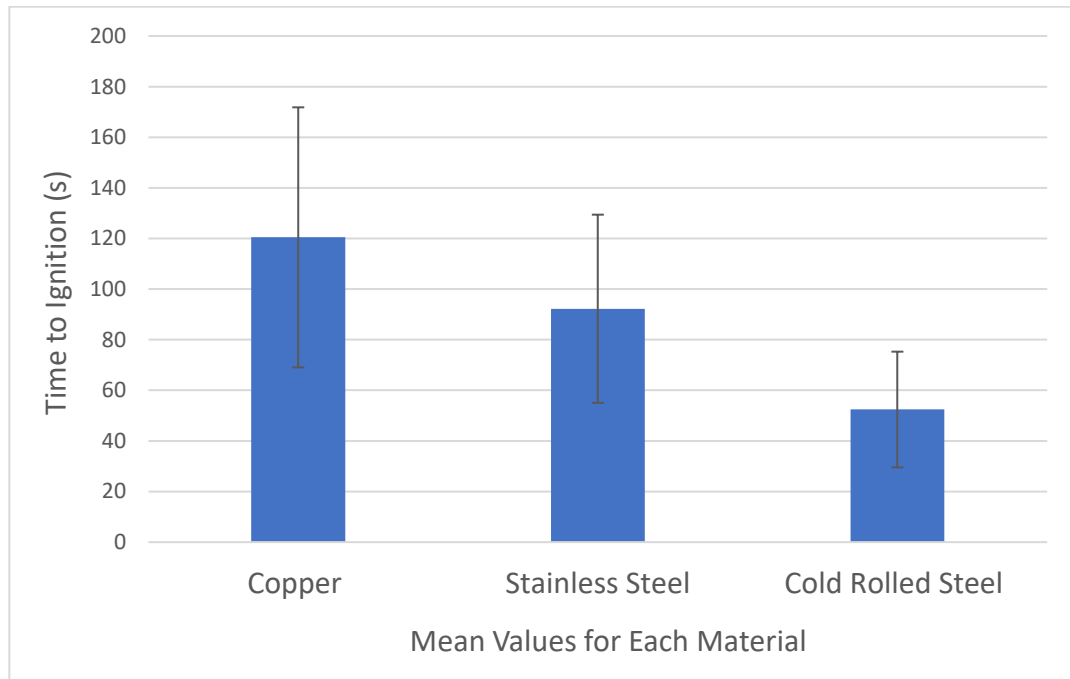


**Figure 4.15** Effects of Metallic Sparks on Mean Time to Ignition for Cheatgrass Fuel. Error bars indicate the standard error multiplied by the respective t-value of the observed data.

### 4.3.5 Class SS/CR-Th

The final class of these experiments studied the interaction of the same metals (*i.e.*, stainless steel and cold rolled steel) with Timothy hay fuel. From Figure 4.16, we concluded that cold rolled steel was the most successful metal in igniting all three different fuels with varying fuel moistures. It was observed that only two out of 54 total experiments resulted in ignition (one smolder and one flaming) by stainless steel, while 22 out of 54 total experiments ignited from combinations with cold rolled steel. In addition, most of the

experiments ignited with ambient temperatures above 29 °C (Figure 4.17). Out of seven

experiments conducted under 29 °C, only two ignited. However, thirteen experiments were

run with an ambient temperature above 29 °C, of which 54 % ignited.
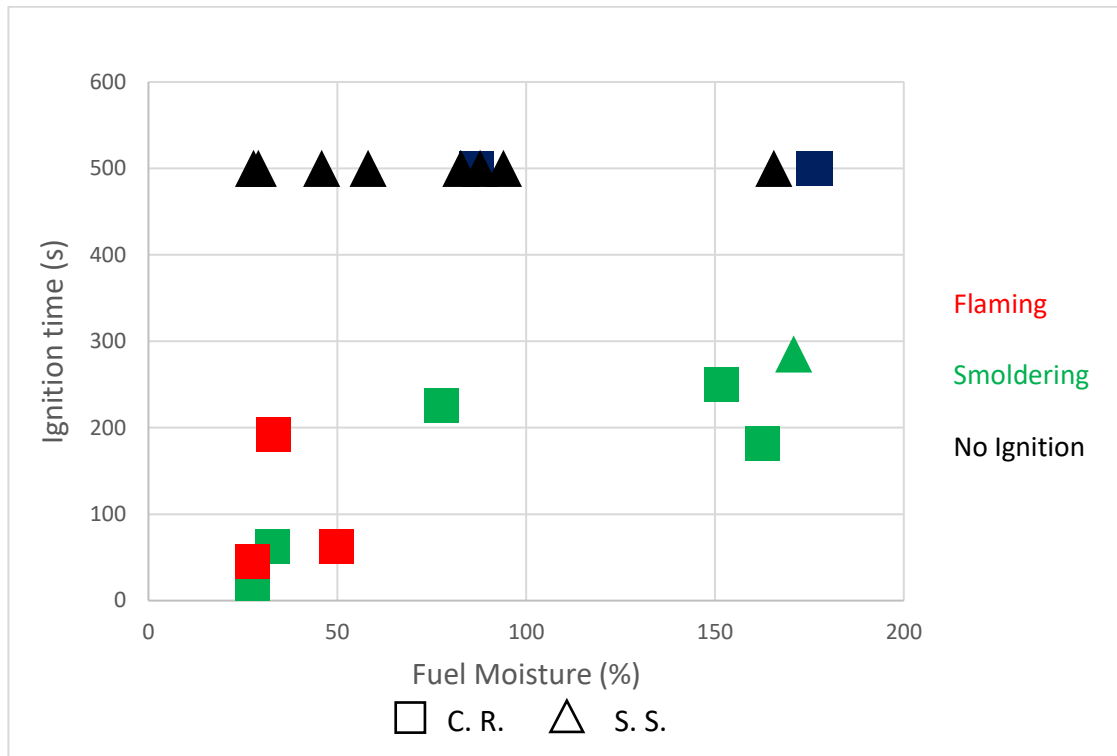


**Figure 4.16** Fuel Moisture vs. Ignition Time for Class SS/CR-Th. Fuel moisture vs. ignition time for soaked Timothy hay fuel in combination with Cold Rolled Steel (Square) and Stainless (Triangle). Showing flaming ignition (red), smoldering ignition (green) and no ignition (black). Corresponding dry times of 1 hour (smallest shape/icon), 2 hours (largest shape/icon), and 3 hours (median shape/icon).
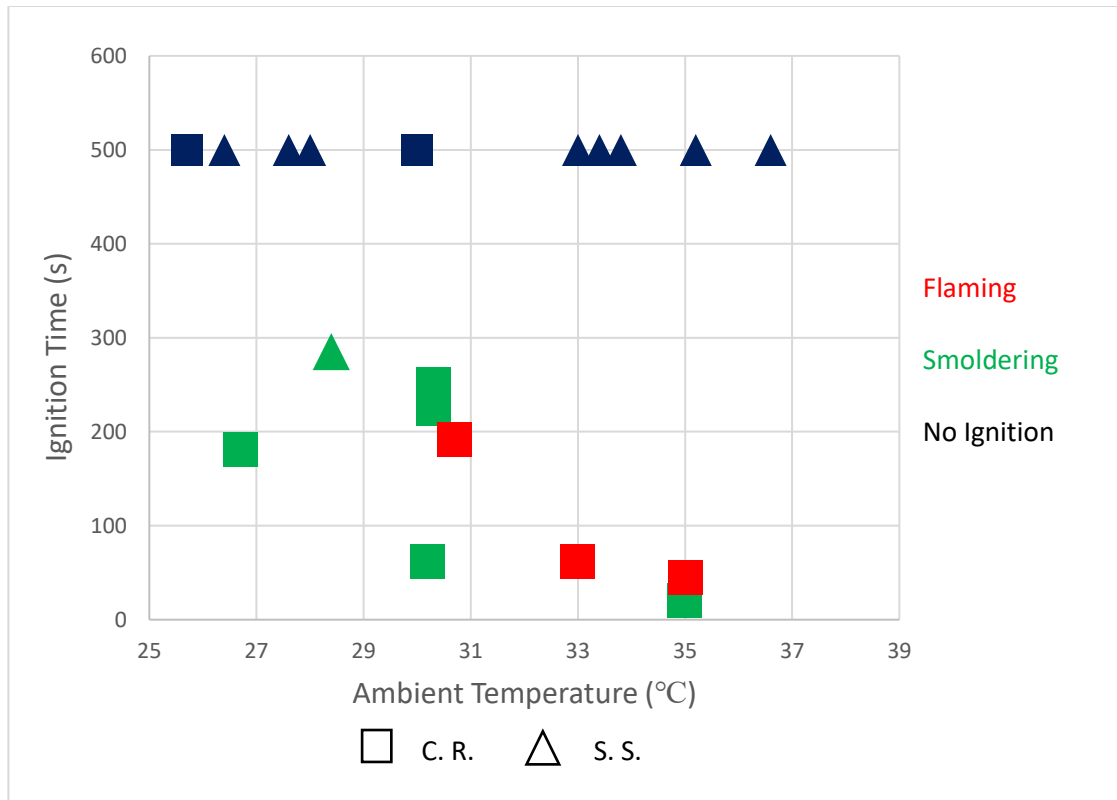
**Figure 4.17** Ambient Temperature vs. Time for Class SS/CR-Th. Ambient temperature vs. ignition time for soaked Timothy hay fuel in combination with Cold Rolled Steel (Square) and Stainless (Triangle). Showing flaming ignition (red), smoldering ignition (green) and no ignition (black). Corresponding dry times of 1 hour (smallest shape/icon), 2 hours (largest shape/icon), and 3 hours (median shape/icon).

### 4.3.6  Statistical Analysis of Mean Ignition Times for Class SS/CR-Th

This section provides the calculated mean and standard deviation for each sample of set 2 using student's t-value distribution. Figure 4.18 list the mean ignition times with corresponding error bars. The error bars consist of the sample standard error multiplied by the t-value.
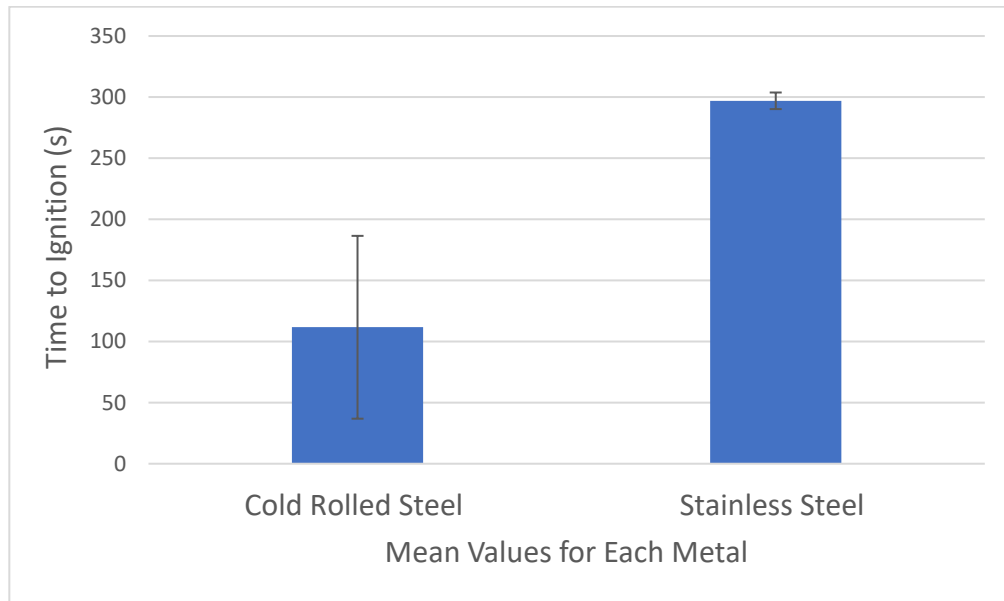


**Figure 4.18** Effects of Metallic Sparks on Mean Time to Ignition for Timothy Fuel. Error bars indicate the standard error multiplied by the respective t-value of the observed data.

# 4.4 Results of Set 3 Experiments - Varying Distance Experiments

Class CR is separated into two categories: (1) smaller distances (40 cm, 50 cm, and 60 cm) and (2) greater distances (80 cm, and 100 cm). Out of 54 total experiments conducted in set 2, stainless steel produced a total of two ignitions, and cold rolled steel resulted in a total of 22 ignitions. Therefore, it was determined that cold rolled steel possess the higher ignition capability amongst both metals.

## 4.4.1 Class CR-Cg-1

Class CR-Cg studied the interaction of Cheatgrass fuel with Cold Rolled Steel at three different height distances: 40 cm, 50 cm, and 60 cm. Unlike the previous classes, Class CR-Cg focuses on more realistic distances found in real life grinding scenarios. Successful flaming ignition was observed to be 83 % (10 of 12 total experiments), where 40 % transitioned from smoldering to flaming ignition. Most experiments ignited within 20 to 40 seconds with an average ignition flaming time of 41 seconds. From Figure 4.20, we can see that for distances of 40 cm and 50 cm, 100 % ignition was observed. However, for distances of 60 cm, a probability of 67% for ignitions was observed, with half of those consisting of a smoldering to flaming ignition transition.

## 4.4.2 Class CR-Cg-2 (Distances of 80 and 100 cm)

Experiments in this class differ from the previous by changing the distance from the fuel bed to the grinder to 80 cm and 100 cm. Successful flaming ignition was observed to be 71 % (10 of 14 total experiments) of which 60 % transitioned from smoldering to flaming ignition. Smoldering ignition was observed for the remaining four experiments

but never transitioned to flaming ignition. The main point of interest is that intuitively we would expect that the greater distances (80 and 100 cm) would take a longer time to ignite the fuel when compared to that of the lesser distances (40, 50, and 60 cm). The reasoning behind this is that the particle would have to travel a greater distance for a longer period, all while experiencing greater heat losses than when traveling a shorter distance. From Figure 4.20, we can see that for ambient temperatures less than 40 ℃, the greater distances of 80 cm and 100 cm do indeed take longer to ignite when compared to the smaller distances. However, for ambient temperatures ranging higher than 40 ℃, we can see that the greater distances (80 cm and 100 cm) ignite at relatively similar times of that of the smaller distances (40 cm, 50 cm, and 60 cm). It was observed that the one major difference was that the ambient temperature was much higher when running the greater distances for that day. This, in turn, reduced the heat loss of the particles via convection and radiation. This reduction in heat loss to the particle's surroundings allowed the particle to reach the fuel bed with a higher thermal energy and ignited it at a faster rate.
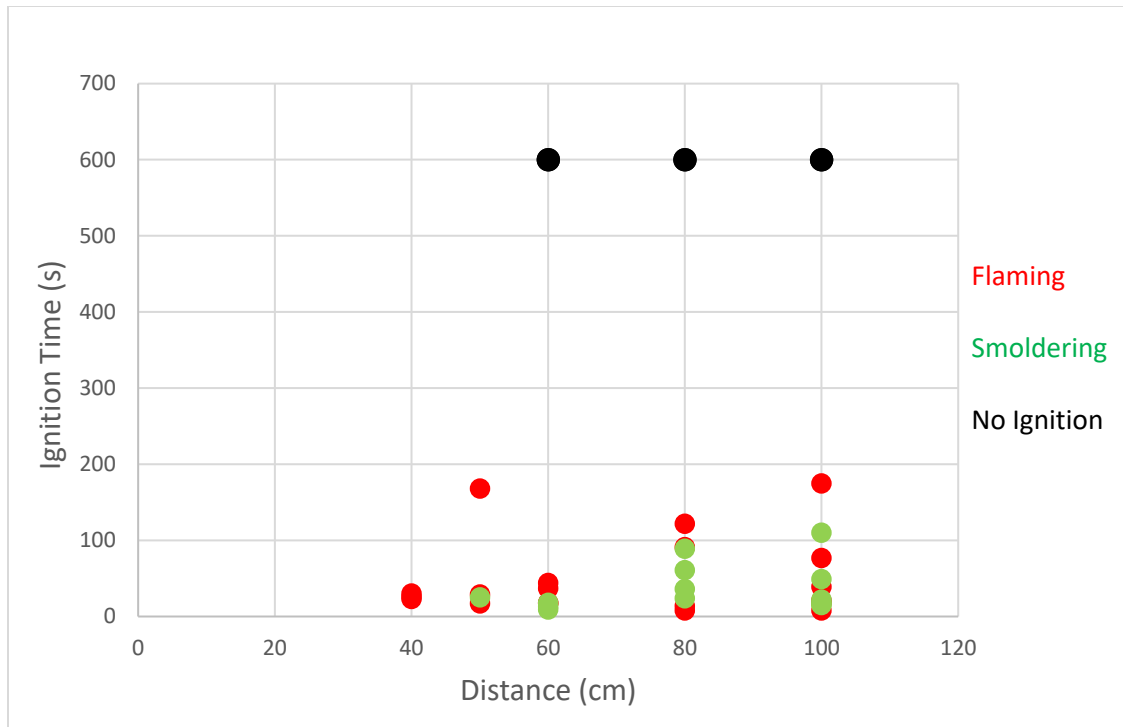
**Figure 4.19** Comparison of All Distances (40, 50, 60, 80, and 100 cm) vs. Ignition Time for Class CR-Cg. All distances vs. ignition time for oven dried Cheatgrass fuel in combination with Cold Rolled Steel. Showing flaming ignition (red), smoldering ignition (green) and no ignition (black).
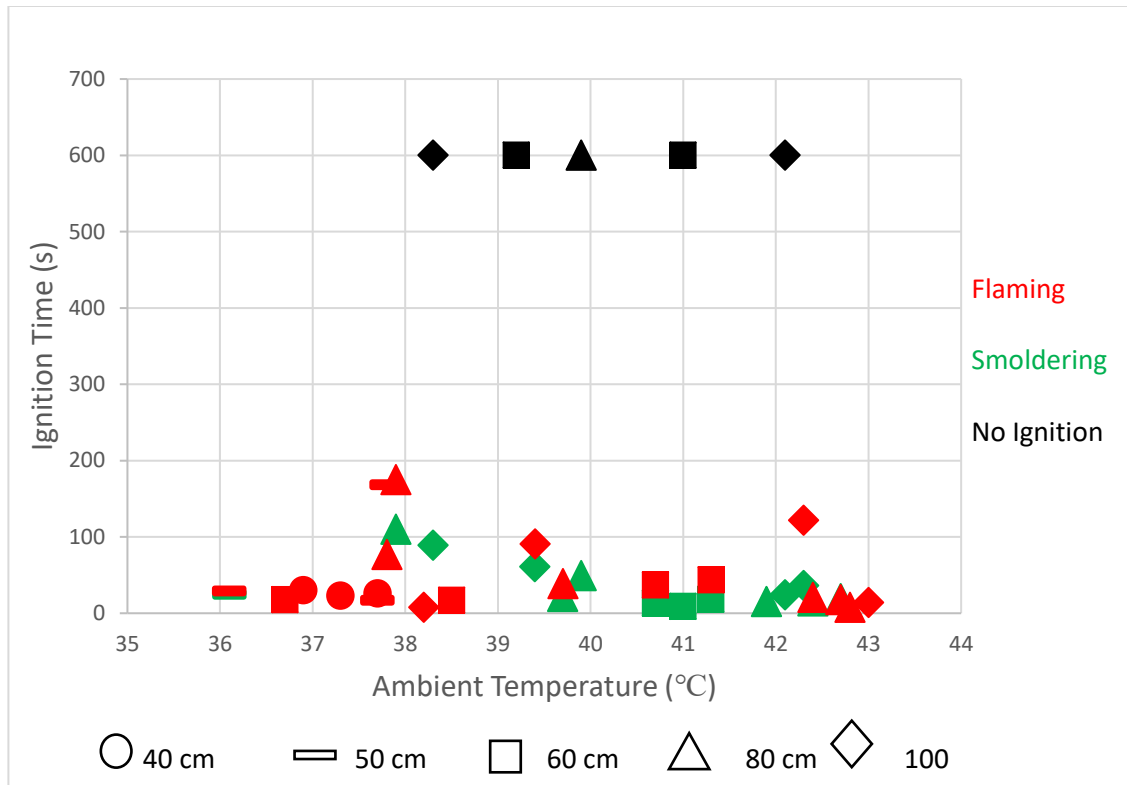
**Figure 4.20** Ambient Temperature vs. Ignition Time for All Distances for Class CR-Cg. Ambient Temperature vs. ignition time for oven dried Cheatgrass fuel in combination with Cold Rolled Steel. Showing flaming ignition (red), smoldering ignition (green) and no ignition (black). Distance corresponding shapes: 40 cm (circle), 50 cm (rectangle), 60 cm (square), 80 cm (diamond), and 100 cm (triangle).

### 4.4.3  Statistical Analysis of Mean Ignition Times for Class CR-Cg

This section provides the calculated mean and standard deviation for each sample of set 3 using student's t-value distribution. Figure 4.21 list the mean ignition times with corresponding error bars. The error bars consist of the sample standard error multiplied by the t-value.
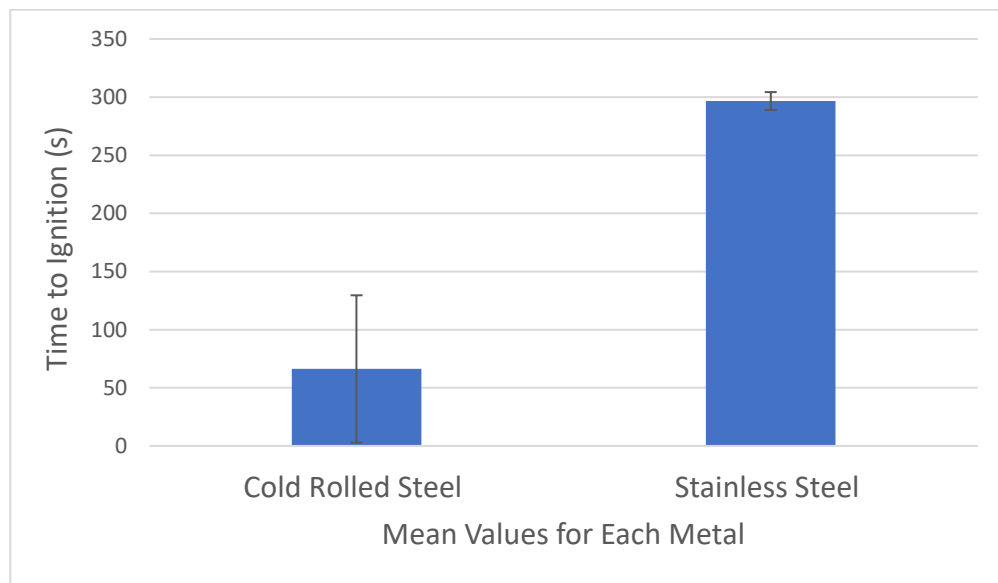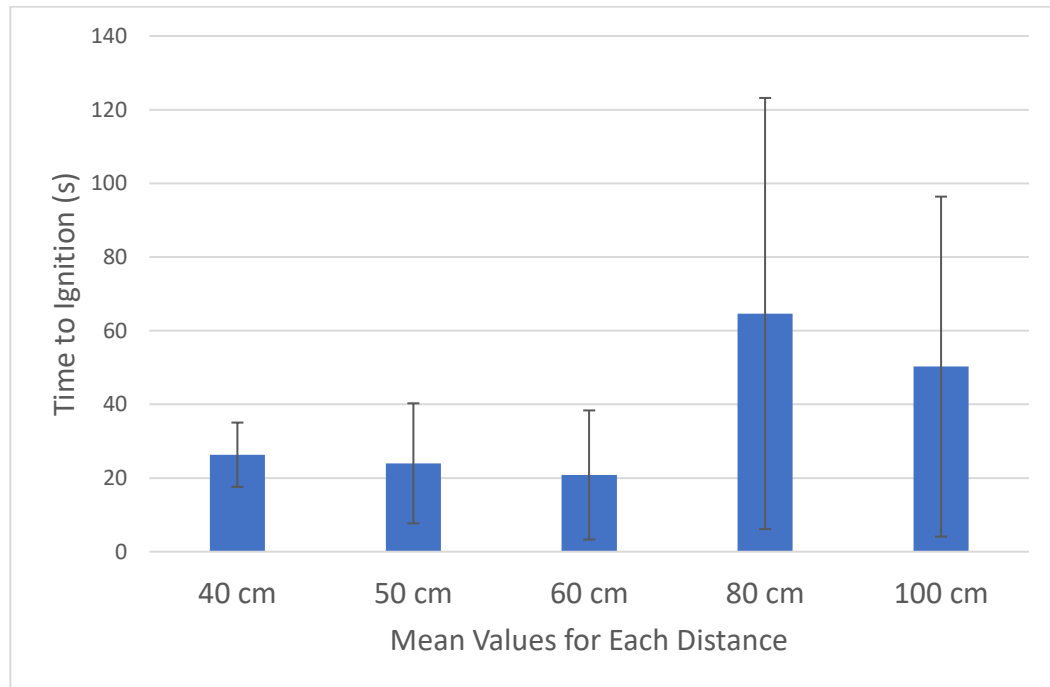


**Figure 4.21** Effect of Distance on Mean Time to Ignition of Cold Rolled Steel in combination with Cheatgrass Fuel for Set 3. Error bars indicate the standard error multiplied by the respective t-value of the observed data.

## 4.5 Modification of Transient Energy Equation

From the results, it is hypothesized that a new term must be added to the transient energy equation used to calculate the temperature ($T_P$) of a metal sphere particle. The original energy equation presented in section 3.2 (Equation 1) takes into account convective and radiative energy losses. In section 3.2, it was presented that radiative heat losses can be neglected, and the final temperature of the particle may be found solely based on the convective energy losses. However, the experimental results presented in the previous chapter indicate that that is applicable only to copper and can not be used to calculate the final temperature of a particle for neither cold rolled steel or stainless-steel. Due to the cold rolled steel and stainless-steel metal particles combusting, a term that accounts for the reaction energy released must be added. This is proposed, since an exothermic oxidation reaction takes place and combustion of the metal particles occurs. Therefore, the energy equation (equation 1 from section 3.2) becomes:

$$V_p c_p \left(\frac{dT_P}{dt}\right) = \left(hA_p(T_P - T_\infty) + \sigma \varepsilon A_p(T_P^4 - T_\infty^4)\right) + \Delta H_{reaction} \qquad (23)$$

where $\Delta H_{reaction}$ is the energy released during particle combustion. The details of this analysis are out of the scope of this thesis and are given as a part of the fuel report to the Forest Service. The combustion of stainless and cold rolled steel particles is also supported by the microscopic images discussed in the following section.

# 4.6 Results of Particle Imaging

The found particle sizes of cold rolled steel were in the following range: 0.0625 mm - 0.75 mm. As explained in the grinding physical process section, Behrend and Ritter (2004) summarized that materials with a higher toughness generated smaller particles and materials with a lower toughness created larger particles, since the material can be easily deformed. From Table 3.1, we can see that cold rolled steel has the highest yield tensile strength followed by stainless steel and lastly copper. From this, we can infer that cold rolled steel would create the smallest particles and copper would generate the largest particles.

This is supported by our findings that the typical particle diameter range for cold rolled steel was from 0.0625 mm - 0.75 mm and was much about 10x smaller when compared to that of copper which ranged from 0.4375 mm – 2.5 mm (Table 4.4). It must be noted that diameter size of 0.0625 mm was dominant for cold rolled steel, but larger particles were observed as well. Table A.4 may be found in Appendix A which lists multiple samples with a variety of diameter size measured.

**Table 4.4** Particle Diameter Range

| Metal | Diameter (mm) |
|---|---|
| Stainless Steel | 0.0625 – 0.80 |
| Cold Rolled Steel | 0.0625 – 0.80 |
| Copper | 0.4375 – 2.5 |

From the microscopic image of cold rolled steel (Figure 4.22a), we can see that the difference in particle sizes is significant when compared to that of the microscopic image of copper (Figure 4.22c).
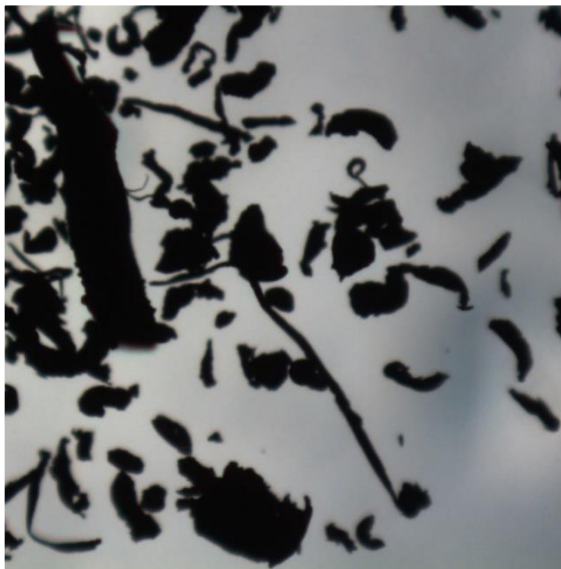
**Figure 4.22** Microscopic images of a.) Cold Rolled Steel, b.) Stainless Steel, c.) Copper, and d.) Aluminum.

In Figures 4.22a, and 4.22b, we notice the presence of smaller spherical shape particles. Conversely, in Figures 4.22c and 4.22d, larger irregular particles are seen. This leads us to our second finding which agrees with the algorithm for determining the transition states of a metal chip (refer to Figure 3.3) proposed by Nikiforov *et al.* 2017.

Nikiforov *et al.* (2017) proposed that when the surface temperature of a metal chip exceeded the oxide's melting point, combustion would occur. They correlated the combustion of metal chips to the sparks we see through the naked eye. This was supported by noting that in the absence of sparks, for metals like copper, no globules are observed. Globules are "the oxidation product of metal particles (chip)" and appear only if particle combustion occurs (Nikiforov *et al.*, 2017). A detailed microscopic image of the sludge (final product after grinding) may be found below in Figure 4.23, which contains globules, chips, and grain fragments.
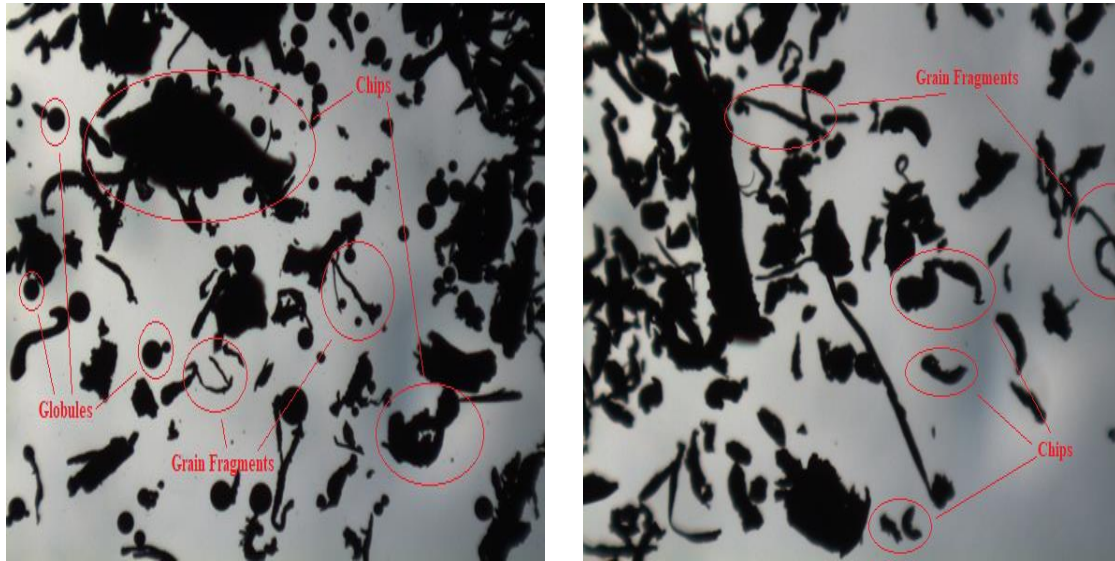
**Figure 4.23** Structure of Grinding Sludge. Following is numbers corresponding to sludge structure for both Cold Rolled Steel (Left) and Copper (Right): (1) globules; (2) chips; (3) grain fragments. (Adopted from Nikiforov *et al.*, 2017)

By the following the algorithm (Refer to Figure 3.3) and using Nikiforov hypothesis, we may safely assume the different states of our particles using the microscope images recorded. For example, our findings agreed with Nikiforov hypothesis in that when no sparks are observed for metals such as copper and aluminum, then no globules are present in the sludge (*i.e*., the final product). We can see this in Figures 4.22c and 4.22d, where no globules are present and large metal chips are dominant. Behrend and Ritter (2004) state that "with more ductile metal like aluminum the situation is different. Because of the low melting point of about 660 Celsius and the immediate formation of an oxide layer which prevents further access of oxygen for the initiation of combustion, only liquid metal which drops off without an igniting effect is formed during grinding work". As for copper, larger chip particles are formed due to its low toughness and assumed not to heat sufficiently enough for combustion. It was observed that cold rolled steel and stainless steel possessed

the highest ignition capability, which can be attributed to the combustion of metals chips. This is represented by the dominant globules found in Figures 4.22a and 4.22b. The significance of the globules found in Figures 4.22a and 4.22b., allows us to assume that the metal chips surface temperature exceeded the oxides melting point. This, in turn, caused the particle to combust and further heating the particle before impact with the fuel bed. Lastly, when comparing the cold rolled steel sludge (Figure 4.22a) to that of the stainless-steel sludge (Figure 4.22b), we notice that the quantity of globules appear to be greater for the cold rolled steel sludge. This can be attributed to the differences in carbon percentages found in the two different materials (Table 4.5)

**Table 4.5** Carbon Percentages for each Metal

| Material | Material Grade Selection | Carbon Percentage |
|---|---|---|
| Cold Rolled Steel | AISI 1018 Steel, Cold Drawn | 0.14 – 20 % |
| Stainless Steel | 304 Stainless Steel | $\leq$ .08 % |
| Copper | Copper Bar Alloy  110 | — |

This increase in globules, which implies a greater volume of sparks (refer to Figure 3.4), indicates that the sparks contact area with the fuel is increased for cold rolled steel. Consequently, allowing cold rolled steel to possess a greater ignition capability than stainless steel.

# 5.0 Summary

This thesis has described an experimental apparatus and procedure that was developed to investigate the ignition capability of a shower of metal particles in igniting various wildland fuels. The apparatus allowed the metal workpiece to impact the grinder and deflect the generated shower of sparks onto the fuel bed. The ability to deflect the shower of sparks onto the fuel is important, as it is speculated that the accumulation of energy from multiple particles (sparks) is required for ignition to occur. The metals considered were copper, stainless steel and cold rolled steel and the fuels considered were Lehmann lovegrass, Wild oats, Timothy grass, and Cheatgrass. The parameters varied were the following: fuel temperature, fuel moisture, and distance from the grinder to the fuel bed. The fuel temperature was varied to match that of moderate and hot summer conditions, and the distance was varied to replicate real-life applications.

From the experiments, it was observed that cold rolled steel possessed the highest ignition capability among all three metals. Although copper generated larger size chips, the metal chip's initial temperature was low due to the lower separation energy produced from a ductile material. Cold rolled steel and stainless steel (tougher materials) achieved higher temperatures due to the particles combusting. The microscale size of the particles encouraged for an exothermic oxidation reaction to take place, which allowed the particles to combust and reach higher temperatures. This is supported by the presence of globules (spherical particles) found in the microscopic images, which is an indication that combustion occurred.

The recorded diameter of both the cold rolled steel, and stainless-steel particles generated during the experiments ranged from 0.0625 mm to 0.8 mm. This is important as previous studies focused on particle sizes of 0.8 mm and above, while also stating that any smaller diameters are unlikely to ignite wildland fuels. Their studies also only consisted of analyzing how a single hot sphere particle may ignite fuels. Although a single particle at the microscale size may not ignite the fuel, our work showed that the accumulation of energy from multiple particles impacting the fuel bed will.

It was noted that ambient temperature is imperative on the fuel characteristics, but also has a strong influence on post heat losses. From the post heat loss equations, we can postulate that higher ambient temperature will reduce the heat losses a particle experiences and allow it to lose less thermal energy over time. A lower fuel moisture was also determined to be pivotal in increasing the chances for ignition to occur across all experiments.

Measuring the exact temperature of such a particle at the microscale size is difficult to do, but it can be estimated using the known post heat loss equations and the change in enthalpy of the oxidation reaction. Current work is being conducted to estimate the particle temperature using an analytical model. Furthermore, a logistical regression algorithm using machine learning is being developed to provide a probability of smoldering or flaming ignition based on the recorded data for all sets.

On the basis of these findings, the metal's mechanical properties, size of particles, the temperature of particles and fuel properties are important parameters in determining the ignition propensity of wildland fuels. With the support of other literature studies, it aspires

that these experimental results be used to enhance and validate future analytical and numerical models.

# 6.0 References

Arulmoli, J., Vu, B., Sung, M.-J., Mohamed, F. A., & Earthman, J. C. (2014). Spark production by abrasion of titanium alloys in golf club heads. *Fire and Materials*.

Babrauskas, V. (2003). *Ignition Handbook: principles and applications to fire safety engineering, fire investigation, risk management and forensic science*. Fire Science Publishers.

Behrend, E., & Ritter, K. (2004). Mechanically Generated Sparks. In M. Hattwig & S. Henrikus (Eds.), *Handbook of Explosion Prevention and Protection* (pp. 178–200). Weinheim: WILEY-VCH Verlag GmbH & Co. KGaA.

Brandin, A.-S. (2017). How climate change is increasing forest fires around the world | DW Environment | DW | 19.06.2017. Retrieved December 20, 2017, from http://www.dw.com/en/how-climate-change-is-increasing-forest-fires-around-the-world/a-19465490

CABI. (2017). Bromus tectorum (downy brome). Retrieved December 4, 2017, from https://www.cabi.org/isc/datasheet/10036

Computrac MAX-2000 User â€™ s Manual. (1996), (July 1996).

Di Blasi, C. (1993). Modeling and simulation of combustion processes of charring and non-charring solid fuels. *Progress in Energy and Combustion Science*, *19*(1), 71–104. http://doi.org/10.1016/0360-1285(93)90022-7

Fernandez-Pello, A. C., Lautenberger, C., Rich, D., Zak, C., Urban, J., Hadden, R., … Fereres, S. (2015). Spot fire ignition of natural fuel beds by hot metal particles, embers, and sparks. *Combustion Science and Technology*, *187*(1–2), 269–295. https://doi.org/10.1080/00102202.2014.973953

Finney, M. A., McAllister, S. S., Maynard, T. B., & Grob, I. J. (2016). A Study of Wildfire Ignition by Rifle Bullets. *Fire Technology*, *52*(3), 931–954. http://doi.org/10.1007/s10694-015-0518-6

Hadden, R. M., Scott, S., Lautenberger, C., & Fernandez-Pello, C. C. (2011). Ignition of Combustible Fuel Beds by Hot Particles: An Experimental and Theoretical Study. *Fire Technology*, *47*(2), 341–355. https://doi.org/10.1007/s10694-010-0181-x

Hawksworth, S., Rogers, R., Beyer, M., Proust, C., Lakic, D., Gummer, J., & Raveau, D. (2006). Assessing the potential for ignition from mechanical equipment. *Institution of Chemical Engineers Symposium Series*, (151), 963–971. Retrieved from https://www.scopus.com/inward/record.uri?eid=2-s2.0-33646173212&partnerID=40&md5=55272edf90f388d9b0fe605306f4849c

Howitt, D. G. (2015). An assessment of hot metal fragments from heavy mechanical equipment as a potential ignition source for forest litter. *Journal of Fire Sciences*, *33*(6), 427–444. https://doi.org/10.1177/0734904115611820

Idaho Plant Materials Program, U. (n.d.). Plant guide for Timothy (Phleum pratense). Retrieved from https://plants.usda.gov/plantguide/pdf/pg_phpr3.pdf

Ignition Sources California 2015 (CalFire)
    Retrieved from: cdfdata.fire.ca.gov/incidents/incidents_statsevents

Incropera, F. P., DeWitt, D. P., Bergman, T. L., & Lavine, A. S. (2017). Fundamentals of Heat and Mass Transfer 7th Edition. New York: John Wiley & Sons.

Jain, Mahesh C. (2009). *Textbook of Engineering Physics (Part I)*. *p. 9*. *ISBN* *81-203-3862-6*., Chapter 1, p. 9

Kaminski, G. C. (1974). Ignition Time vs Temperature For Selected Forest Fuels. Retrieved December 20, 2017, from https://www.fs.fed.us/t-d/programs/fire/spark/html/74511201/74511201.html

Lu, L., Farris, T. N., & Chandrasekar, S. (1992). Sliding Microindentation Wear Particles: Spheres in Grinding Swarf. *Tribology Series*, *21*(C), 257–263. http://doi.org/10.1016/S0167-8922(08)70531-5

Manzello, S. L., Cleary, T. G., Shields, J. R., & Yang, J. C. (2006). On the ignition of fuel beds by firebrands. *Fire and Materials*, *30*(1), 77–87. https://doi.org/10.1002/fam.901

Mindykowski, P., Fuentes, A., Consalvi, J. L., & Porterie, B. (2011). Piloted ignition of wildland fuels. *Fire Safety Journal*, *46*(1–2), 34–40. https://doi.org/10.1016/j.firesaf.2010.09.003

National Oceanic and Atmospheric Administration (NOAA). (n.d.). Dead Fuel Moisture | Did You Know? | Monitoring References | National Centers for Environmental Information (NCEI). Retrieved November 30, 2017, from https://www.ncdc.noaa.gov/monitoring-references/dyk/deadfuelmoisture

NDT Education Research Center. (n.d.) Materials and Processes Toughness. Retrieved from https://www.nde-ed.org/EducationResources/CommunityCollege/Materials/Mechanical/Toughness.htm

Nikiforov, I., Maltsev, P., Ivanov, V., & Barsuk, I. (2015). Explanation of the express method of the determination of steel grade by spark. *Environment Technology Resources*, *1*, 157–161.

Nikiforov, I. P., Plokhov, I. V., Mal'tsev, P. N., & Ivanov, V. V. (2017). Chip combustion in metal grinding. *Russin Engineering Research*, *37*(6), 530–535. https://doi.org/10.3103/S1068798X17060156

Pitts, W. M. (2007). *Ignition of Cellulosic Fuel by Heated and Radiative Surfaces*.

Plucinski, M. P., & Anderson, W. R. (2008). Laboratory determination of factors influencing successful point ignition in the litter layer of shrubland vegetation. *International Journal of Wildland Fire*, *17*(5), 628–637. https://doi.org/10.1071/WF07046

Simonin, K. A. (2001). Bromus rubens, Bromus madritensis. Retrieved December 4, 2017, from https://www.fs.fed.us/database/feis/plants/graminoid/brospp/all.html#FIRE ECOLOGY

Tse, S. D., & Fernandez-Pello, A. C. (1998). On the flight paths of metal particles and embers generated by power lines in high winds - a potential source of wildland fires. *Fire Safety Journal*, *30*, 333–356. http://doi.org/10.1016/S0379-7112(97)00050-7

UCIPM. (2016). Weed Gallery: Wild oat--UC IPM. Retrieved December 4, 2017, from http://ipm.ucanr.edu/PMG/WEEDS/wild_oat.html

USDA NRCS Plant Materials Program. (2002). Plants Profile for Eragrostis lehmanniana (Lehmann lovegrass). Retrieved December 4, 2017, from https://plants.usda.gov/core/profile?symbol=ercu2

Wang, L., Mo, S. J., Liang, D., & Yang, W. B. (2013). Research on melted bead ignition capability for the combustible. *Procedia Engineering*, *52*, 386–389. https://doi.org/10.1016/j.proeng.2013.02.157

Weed Gallery: Wild oat--UC IPM. (n.d.). Retrieved December 4, 2017, from http://ipm.ucanr.edu/PMG/WEEDS/wild_oat.html

Yan, H., Simon, D., Vercammen, P., & CNN. (2017). California wildfires have destroyed 1,000 structures ... and counting - CNN. Retrieved December 20, 2017, from http://www.cnn.com/2017/12/11/us/california-wildfires/index.html

Zak, C., Urban, J., Tran, V., & Fernandez-Pello, C. (2014). Flaming ignition behavior of hot steel and aluminum spheres landing in cellulose fuel beds. *Fire Safety Science*, *11*, 1368–1378. https://doi.org/10.3801/IAFSS.FSS.11-1368

Zouhar, K. (2003). Bromus tectorum. Retrieved December 4, 2017, from https://www.fs.fed.us/database/feis/plants/graminoid/brotec/all.html#FireEffects

# Appendix A – Table of Experimental Parameters

The following tables present experimental parameters for all 3 sets of experiments (Table A.1-3). Table A.4 provides multiple particle diameters observed for all samples.

**Table A.1** Parameters Measured for Set 1 at a set distance of 10 cm

| Experiment Number | Ambient Temp (°C) | Relative Humidity | Metal Material | Fuel Type | Dead Fuel Moisture | Smoldering Time | Flaming Time | Fuel Temp (°C) |
|---|---|---|---|---|---|---|---|---|
| 41 | 27.9 | 0.18 | Stainless steel | Lovegrass | 4.45% | not visible | 0:18 | 27.94 |
| 42 | 28.5 | 0.16 | stainless steel | WILDOATS | 5.19% | NA | 4:15 | 28.50 |
| 43 | 27.3 | 0.16 | Stainless steel | Timothy | 2.03% | 4:40 | 5:20 | 27.33 |
| 44 | 27.1 | 0.17 | ColdRod steel | Lovegrass | 4.45% | NA | 3:30 | 27.11 |
| 45 | 27.3 | 0.15 | ColdRod steel | WILDOATS | 5.19% | NA | 0:42 | 27.28 |
| 46 | 27.7 | 0.16 | ColdRod steel | Timothy | 2.03% | 0:18 | 0:24 | 55.00 |
| 47 | 26.6 | 0.25 | stainless steel | Lovegrass | 4.09% | NA | NA | 26.56 |
| 48 | 26.0 | 0.27 | stainless steel | WILDOATS | 5.59% | NA | 0:26 | 45 |
| 49 | 25.6 | 0.27 | ColdRod steel | WILDOATS | 5.59% | 0:36 | 0:42 | 45 |
| 50 | 24.4 | 0.18 | copper | Lovegrass | 4.45% | 47s | NA | 24.44 |
| 51 | 24.4 | 0.18 | copper | WILDOATS | 5.19% | NA | NA | 24.44 |
| 52 | 24.8 | 0.18 | copper | timothy | 2.10% | 1:20 | NA | 24.44 |
| 53 | 25.7 | 0.16 | stainless steel | timothy | 4.35% | 2:30 | 3:25 | 40 |
| 54 | 25.7 | 0.16 | ColdRod steel | Lovegrass | 3.62% | NA | 1:15 | 40 |
| 55 | 25.7 | 0.16 | copper | Lovegrass | 3.62% | 4:30 | NA | 40 |
| 56 | 26.9 | 0.15 | ColdRod steel | timothy | 4.35% | 0:15 | 0:24 | 40 |
| 57 | 26.7 | 0.15 | copper | timothy | 4.35% | 2:25 | NA | 40 |
| 58 | 27.2 | 0.15 | copper | WILDOATS | 3.92% | 2:10 | NA | 40 |

84

| 59 | 28.8 | 0.17 | copper | Lovegrass | 2.92% | NA | NA | 55 |
|---|---|---|---|---|---|---|---|---|
| 60 | 30.6 | 0.18 | stainless steel | WILDOATS | 2.93% | NA | 3:00 | 55 |
| 61 | 29.2 | 0.18 | ColdRod steel | timothy | 3.20% | 0:15 | 1:00 | 55 |
| 62 | 29.0 | 0.17 | stainless steel | Lovegrass | 2.92% | NA | 2:10 | 55 |
| 63 | 29.2 | 0.17 | ColdRod steel | WILDOATS | 2.93% | NA | 1:05 | 55 |
| 64 | 29.5 | 0.17 | stainless steel | timothy | 3.20% | 0:15 | 1:02 | 55 |
| 65 | 29.6 | 0.17 | copper | WILDOATS | 2.92% | 1:30 | NA | 55 |
| 66 | 30.9 | 0.17 | copper | timothy | 3.20% | 1:27 | NA | 55 |
| 67 | 29.6 | 0.17 | ColdRod steel | Lovegrass | 2.92% | 0:15 | NA | 55 |
| 68 | 30.9 | 0.17 | stainless steel | Lovegrass | 5.43% | NA | 1:18 | 30.89 |
| 69 | 30.6 | 0.17 | stainless steel | WILDOATS | 6.03% | NA | 2:44 | 30.56 |
| 70 | 30.6 | 0.17 | ColdRod steel | Lovegrass | 5.43% | NA | 0:45 | 30.56 |
| 71 | 29.6 | 0.17 | ColdRod steel | WILDOATS | 6.03% | 0:54 | 1:10 | 29.56 |
| 72 | 29.0 | 0.17 | copper | Lovegrass | 5.43% | 3:00 | 3:00 | 29 |
| 73 | 28.9 | 0.17 | copper | WILDOATS | 6.03% | NA | NA | 28.89 |
| 74 | 28.8 | 0.25 | stainless steel | timothy | 3.20% | slight | NA | 28.78 |
| 75 | 27.7 | 0.25 | ColdRod steel | timothy | 3.20% | 3:40-5:25 | NA | 27.67 |
| 76 | 28.8 | 0.25 | copper | timothy | 3.20% | 6:00-8:09 | NA | 28.78 |
| 77 | 28.9 | 0.23 | stainless steel | Lovegrass | 3.82% | NA | 4:11 | 40 |
| 78 | 29.4 | 0.21 | ColdRod steel | WILDOATS | 4.07% | NA | 1:57 | 40 |
| 79 | 29.1 | 0.2 | copper | timothy | 3.20% | 4:50 | NA | 40 |
| 80 | 29.0 | 0.2 | copper | Lovegrass | 3.82% | 4:20 | NA | 40 |
| 81 | 29.2 | 0.24 | stainless steel | WILDOATS | 4.07% | NA | 0:40 | 40 |
| 82 | 29.2 | 0.22 | ColdRod steel | Timothy | 3.20% | NA | 0:25 | 40 |

| | | | | | | | | |
|---|---|---|---|---|---|---|---|---|
| 83 | 28.8 | 0.23 | ColdRod steel | Lovegrass | 3.82% | NA | 0:20 | 40 |
| 84 | 29.2 | 0.26 | stainless steel | Timothy | 3.20% | NA | 0:23 | 40 |
| 85 | 29.2 | 0.26 | copper | WILDOATS | 4.07% | NA | NA | 40 |
| 86 | 30.3 | 0.16 | stainless steel | Lovegrass | 2.25% | NA | 2:00 | 55 |
| 87 | 30.1 | 0.16 | ColdRod steel | WILDOATS | 3.14% | NA | 2:35 | 55 |
| 88 | 30.7 | 0.16 | Coldrod steel | Timothy | 1.60% | 0:15 | 0:25 | 55 |
| 89 | 31.2 | 0.15 | ColdRod steel | Lovegrass | 2.25% | NA | 0:10 | 55 |
| 90 | 31.4 | 0.17 | stainless steel | WILDOATS | 3.14% | NA | 0:41 | 55 |
| 91 | 31.6 | 0.16 | stainless steel | Timothy | 1.60% | NA | NA | 55 |
| 92 | 31.8 | 0.17 | stainless steel | Lovegrass | 5.10% | NA | 0:26 | 33 |
| 93 | 31.8 | 0.18 | cold rod | WILDOATS | 4.58% | NA | 0:11 | 31.78 |
| 94 | 31.7 | 0.2 | cold rod | Timothy | 3.30% | 0:18 | 0:22 | 31.67 |
| 95 | 31.3 | 0.2 | cold rod | Lovegrass | 5.10% | NA | 0:24 | 39 |
| 96 | 31.4 | 0.2 | stainless steel | WILDOATS | 4.58% | NA | NA | 31.44 |
| 97 | 31.6 | 0.2 | stainless steel | timothy | 3.30% | 3:13-3:28 | 3:29 | 31.56 |
| 98 | 31.3 | 0.24 | copper | Lovegrass | 5.10% | NA | NA | 55 |
| 99 | 30.7 | 0.23 | copper | Timothy | 3.30% | NA | NA | 55 |
| 100 | 30.8 | 0.23 | copper | WILDOATS | 4.58% | NA | NA | 55 |
| 101 | 29.3 | 0.16 | copper | timothy | 3.53% | 170 sec | NA | 40 |
| 102 | 29.3 | 0.15 | stainless steel | Lovegrass | 4.36% | NA | 59 | 40 |
| 103 | 28.8 | 0.15 | Ss | WILDOATS | 4.14% | NA | 85 sec | 40 |
| 104 | 29.0 | 0.15 | Ss | timothy | 3.53% | 105 sec | 195 sec | 40 |
| 105 | 29.7 | 0.18 | cold rod | Lovegrass | 4.36% | NA | 25 sec | 40 |
| 106 | 29.2 | 0.19 | cold rod | WILDOATS | 4.14% | NA | 18 sec | 40 |
| 107 | 29.3 | 0.19 | cold rod | timothy | 3.53% | 20 sec | 25 sec | 40 |
| 108 | 28.9 | 0.19 | Ss | Lovegrass | 2.44% | NA | 12 sec | 55 |

| 109 | 29.4 | 0.18 | SS | WILDOATS | 2.50% | NA | 9 sec | 55 |
|---|---|---|---|---|---|---|---|---|
| 110 | 29.1 | 0.18 | SS | timothy | 2.21% | NA | na | 55 |
| 111 | 30.2 | 0.18 | cold rod | Lovegrass | 2.44% | NA | 16 sec | 55 |
| 112 | 30.3 | 0.17 | cold rod | timothy | 2.21% | 20 sec | 25 sec | 55 |
| 113 | 29.7 | 0.19 | cold rod | WILDOATS | 2.50% | NA | 20 sec | 55 |
| 114 | 29.2 | 0.19 | copper | timothy | 2.21% | 2:20-4:45 | NA | 55 |

**Table A.2** Parameters Measured in Set 2

| Experiment Number | Ambient Temp (Celsius) | Relative Humidity | Metal Material | Fuel Type | Fuel Moisture | Smoldering Time | Flame Time | Dry Time |
|---|---|---|---|---|---|---|---|---|
| 1 | 35.9 | 0.35 | C.R. | Aveena Wild oats | 98.71 | 0:01:10 | NA | 1 |
| 2 | 36.9 | 0.33 | C.R. | Aveena Wild oats | 68.90 | 0:01:08 | NA | 2 |
| 3 | 37.6 | 0.33 | C.R. | Aveena Wild oats | 69.14 | NA | 0:00:54 | 2 |
| 4 | 37.9 | 0.31 | C.R. | Aveena Wild oats | 75.52 | 0:00:38 | 0:01:25 | 2 |
| 5 | 32.0 | 0.49 | S.S. | Timothy | 146.47 | NA | NA | 1 |
| 6 | 33.0 | 0.44 | S.S. | Bromus | 83.63 | NA | NA | 1 |
| 7 | 33.8 | 0.43 | S.S. | Timothy | 93.97 | NA | NA | 2 |
| 8 | 33.3 | 0.43 | C.R. | Bromus | 21.48 | NA | 0:00:57 | 2 |
| 9 | 34.6 | 0.42 | S.S. | Bromus | 24.01 | NA | NA | 2 |
| 10 | 35.2 | 0.4 | S.S. | Timothy | 45.84 | NA | NA | 3 |
| 11 | 32.7 | 0.41 | S.S. | Aveena Wild oats | 121.12 | NA | NA | 1 |
| 12 | 33.3 | 0.4 | C.R. | Bromus | 90.86 | 0:03:40 | NA | 1 |
| 13 | 34.3 | 0.38 | S.S. | Aveena Wild oats | 59.44 | NA | NA | 2 |
| 14 | 35.7 | 0.3 | S.S. | Aveena Wild oats | 24.19 | NA | 0:05:00 | 3 |
| 15 | 35.8 | 0.25 | C.R. | Bromus | 12.38 | NA | 0:01:17 | 3 |
| 16 | 30.3 | 0.47 | C.R. | Timothy | 151.83 | 0:04:10 | NA | 1 |
| 17 | 33.0 | 0.38 | C.R. | Timothy | 49.84 | NA | Yes 0:01:02 | 2 |
| 18 | 35.0 | 0.25 | C.R. | Timothy | 27.69 | 0:00:20 | 0:00:45 | 3 |
| 19 | 36.1 | 0.25 | S.S. | Bromus | 10.86 | NA | NA | 3 |
| 20 | 36.4 | 0.25 | C.R. | Aveena Wild oats | 15.49 | NA | NA | 3 |
| 21 | 36.6 | 0.25 | S.S. | Timothy | 27.79 | NA | NA | 3 |

| 22 | 25.7 | 0.57 | C.R. | Timothy | 176.06 | NA | NA | 1 |
|----|------|------|------|---------|--------|----|----|---|
| 23 | 27.6 | 0.51 | S.S. | Bromus | 62.42 | NA | NA | 1 |
| 24 | 30.3 | 0.47 | C.R. | Timothy | 77.52 | 0:03:45 | NA | 2 |
| 25 | 29.8 | 0.46 | S.S. | Bromus | 25.16 | NA | NA | 2 |
| 26 | 30.7 | 0.43 | C.R. | Timothy | 32.97 | 0:01:02 | 0:03:12 | 3 |
| 27 | 30.7 | 0.41 | S.S. | Bromus | 15.49 | NA | NA | 3 |
| 28 | 26.4 | 0.49 | S.S. | Timothy | 165.59 | NA | NA | 1 |
| 29 | 27.7 | 0.45 | C.R. | Aveena Wild oats | 83.35 | NA | NA | 1 |
| 30 | 27.6 | 0.42 | S.S. | Timothy | 82.73 | NA | NA | 2 |
| 31 | 28.0 | 0.4 | S.S. | Timothy | 29.11 | NA | NA | 3 |
| 32 | 29.0 | 0.37 | C.R. | Aveena Wild oats | 19.99 | NA | NA | 3 |
| 33 | 26.8 | 0.53 | S.S. | Aveena Wild oats | 115.12 | NA | NA | 1 |
| 34 | 26.9 | 0.5 | C.R. | Bromus | 68.46 | NA | NA | 1 |
| 35 | 28.6 | 0.45 | S.S. | Aveena Wild oats | 126.02 | NA | NA | 2 |
| 36 | 29.6 | 0.41 | C.R. | Bromus | 56.25 | 0:03:00 | No | 2 |
| 37 | 30.4 | 0.37 | S.S. | Aveena Wild oats | 19.07 | No | No | 3 |
| 38 | 30.8 | 0.36 | C.R. | Bromus | 12.99 | NA | 0:01:02 | 3 |
| 39 | 23.6 | 0.65 | C.R. | Timothy | 176.71 | No | No | 1 |
| 40 | 25.6 | 0.59 | S.S. | Aveena Wild oats | 118.43 | No | No | 1 |
| 41 | 26.7 | 0.57 | C.R. | Timothy | 162.56 | 0:03:01 | No | 2 |
| 42 | 27.3 | 0.53 | S.S. | Aveena Wild oats | 64.77 | No | No | 2 |
| 43 | 30.0 | 0.51 | C.R. | Timothy | 86.76 | No | No | 3 |
| 44 | 30.7 | 0.47 | S.S. | Aveena Wild oats | 35.86 | No | No | 3 |
| 45 | 27.4 | 0.52 | C.R. | Aveena Wild oats | 135.64 | No | No | 1 |
| 46 | 28.4 | 0.49 | S.S. | Timothy | 170.90 | 0:04:45 | No | 1 |
| 47 | 29.9 | 0.45 | C.R. | Aveena Wild oats | 23.99 | No | 0:00:46 | 2 |
| 48 | 33.0 | 0.42 | S.S. | Timothy | 87.84 | No | No | 2 |
| 49 | 32.5 | 0.39 | C.R. | Aveena Wild oats | 15.08 | No | 0:02:24 | 3 |
| 50 | 33.4 | 0.38 | S.S. | Timothy | 58.17 | No | No | 3 |
| 51 | 35.6 | 0.37 | S.S. | Bromus | 89.69 | No | No | 1 |
| 52 | 35.9 | 0.3 | C.R. | Bromus | 90.62 | No | No | 1 |
| 53 | 38.2 | 0.28 | S.S. | Bromus | 13.52 | No | No | 2 |
| 54 | 39.7 | 0.24 | C.R. | Bromus | 8.85 | No | No | 2 |
| 55 | 40.0 |  | S.S. | Bromus | 8.45 | No | No | 3 |
| 56 | 40.4 | 0.22 | C.R. | Bromus | 7.67 | No | No | 3 |

**Table A.3** Parameters Measured in Set 3

| Experiment Number | Ambient Temp. (Celsius) | Relative Humidity | Metal Material | Fuel Type | Smolder Time | Flaming Time | Distance from Fuel to Grinder |
|---|---|---|---|---|---|---|---|
| 1 | 36.1 | 0.31 | C.R. | Bromus | 0:00:25 | 0:00:29 | 50 |
| 2 | 37.7 | 0.26 | C.R. | Bromus | NA | 0:00:17 | 50 |
| 3 | 37.8 | 0.28 | C.R. | Bromus | No | 0:02:48 | 50 |
| 4 | 38.5 | 0.26 | C.R. | Bromus | NA | 0:00:17 | 60 |
| 5 | 39.2 | 0.25 | C.R. | Bromus | NA | | 60 |
| 6 | 36.7 | 0.30 | C.R. | Bromus | No | 0:00:18 | 60 |
| 7 | 36.9 | 0.32 | C.R. | Bromus | NA | 0:00:30 | 40 |
| 8 | 37.7 | 0.30 | C.R. | Bromus | NA | 0:00:26 | 40 |
| 9 | 37.3 | 0.31 | C.R. | Bromus | NA | 0:00:23 | 40 |
| 10 | 37.8 | 0.27 | C.R. | Bromus | NA | 0:01:17 | 100 |
| 11 | 37.9 | 0.28 | C.R. | Bromus | 0:01:50 | 0:02:55 | 100 |
| 12 | 39.9 | 0.27 | C.R. | Bromus | 0:00:49 | No | 100 |
| 13 | 42.3 | 0.22 | C.R. | Bromus | 0:00:36 | 0:02:02 | 80 |
| 14 | 42.1 | 0.21 | C.R. | Bromus | 0:00:24 | No | 80 |
| 15 | 43 | 0.21 | C.R. | Bromus | No | 0:00:14 | 80 |
| 16 | 42.8 | 0.22 | C.R. | Bromus | No | 0:00:08 | 100 |
| 17 | 42.4 | 0.19 | C.R. | Bromus | 0:00:16 | 0:00:21 | 100 |
| 18 | 42.7 | 0.19 | C.R. | Bromus | 0:00:19 | 0:00:18 | 100 |
| 19 | 38.2 | 0.22 | C.R. | Bromus | NA | 0:00:08 | 80 |
| 20 | 38.3 | 0.22 | C.R. | Bromus | 0:1:29 and 0:3:30 | NA | 80 |
| 21 | 39.4 | 0.21 | C.R. | Bromus | 0:01:01 | 0:01:31 | 80 |
| 22 | 39.7 | 0.21 | C.R. | Bromus | 0:00:22 | 0:00:39 | 100 |
| 23 | 41.0 | 0.21 | C.R. | Bromus | 0:00:09 | NA | 60 |
| 24 | 40.7 | 0.22 | C.R. | Bromus | 0:00:13 | 0:00:37 | 60 |
| 25 | 41.3 | 0.21 | C.R. | Bromus | 0:00:18 | 0:00:44 | 60 |
| 26 | 41.9 | 0.24 | C.R. | Bromus | 0:00:15 | NA | 100 |

**Table A.4** Multiple Diameter Samples for All Metals

| Metal | Sample | Number | Diameter (mm) |
|---|---|---|---|
| | 14D | 1 | 0.12 |
| | | 2 | 0.1875 |
| | | 3 | 0.0625 |
| | | 4 | 0.125 |
| | | 5 | 0.0625 |
| | | 1 | 0.25 |
| | | 2 | 0.0625 |

| Stainless Steel | 15D | 3 | 0.1875 |
|---|---|---|---|
| | | 4 | 0.125 |
| | | 5 | 0.75 |
| | | 6 | 0.625 |
| | 16D | 1 | 0.3125 |
| | | 2 | 0.0625 |
| | | 3 | 0.25 |
| | | 4 | 0.1875 |
| | | 5 | 0.4375 |
| Cold Rolled Steel | 17D | 1 | 0.0625 |
| | | 2 | 0.25 |
| | | 3 | 0.0625 |
| | | 4 | 0.125 |
| | 18D | 1 | 0.125 |
| | | 2 | 0.0625 |
| | | 3 | 0.25 |
| | | 4 | 0.375 |
| | | 5 | 0.0625 |
| | 19D | 1 | 0.25 |
| | | 2 | 0.4375 |
| | | 3 | 0.25 |
| | | 4 | 0.125 |
| | | 5 | 0.1875 |
| Copper | 20D | 1 | 0.4375 |
| | | 2 | 0.5 |
| | | 3 | 11.5 |
| | | 4 | 0.75 |
| | | 5 | 1.25 |
| | 21D | 1 | 0.75 |
| | | 2 | 0.875 |
| | | 3 | 0.625 |
| | | 4 | 0.3125 |
| | | 5 | 0.75 |
| | 22D | 1 | 0.625 |
| | | 2 | 1.875 |
| | | 3 | 2.5 |
| | | 4 | 0.75 |
| | | 5 | 0.4375 |